

Soft Matter

Accepted Manuscript



This is an *Accepted Manuscript*, which has been through the Royal Society of Chemistry peer review process and has been accepted for publication.

Accepted Manuscripts are published online shortly after acceptance, before technical editing, formatting and proof reading. Using this free service, authors can make their results available to the community, in citable form, before we publish the edited article. We will replace this *Accepted Manuscript* with the edited and formatted *Advance Article* as soon as it is available.

You can find more information about *Accepted Manuscripts* in the [Information for Authors](#).

Please note that technical editing may introduce minor changes to the text and/or graphics, which may alter content. The journal's standard [Terms & Conditions](#) and the [Ethical guidelines](#) still apply. In no event shall the Royal Society of Chemistry be held responsible for any errors or omissions in this *Accepted Manuscript* or any consequences arising from the use of any information it contains.

Dynamics of suspensions of hydrodynamically structured particles: Analytic theory and applications to experiments

Jonas Riest,^{*a} Thomas Eckert,^b Walter Richtering,^b and Gerhard Nägele^a

Received Xth XXXXXXXXXXXX 20XX, Accepted Xth XXXXXXXXXXXX 20XX

First published on the web Xth XXXXXXXXXXXX 200X

DOI: 10.1039/b000000x

We present an easy-to-use analytic toolbox for the calculation of short-time transport properties of concentrated suspensions of spherical colloidal particles with internal hydrodynamic structure, and direct interactions described by a hard-core or soft Hertz pair potential. The considered dynamic properties include self-diffusion and sedimentation coefficients, the wavenumber-dependent diffusion function determined in dynamic scattering experiments, and the high-frequency shear viscosity. The toolbox is based on the hydrodynamic radius model (HRM) wherein the internal particle structure is mapped on a hydrodynamic radius parameter for unchanged direct interactions, and on an existing simulation data base for solvent-permeable and spherical annulus particles. Useful scaling relations for the diffusion function and self-diffusion coefficient, known to be valid for hard-core interaction, are shown to apply also for soft pair potentials. We further discuss extensions of the toolbox to long-time transport properties including the low-shear zero-frequency viscosity and the long-time self-diffusion coefficient. The versatility of the toolbox is demonstrated by the analysis of a previous light scattering study of suspensions of non-ionic PNIPAM microgels [Eckert *et al.*, *J. Chem. Phys.*, 2008, **129**, 124902] in which a detailed theoretical analysis of the dynamic data was left as an open task. By the comparison with Hertz potential based calculations, we show that the experimental data are consistently and accurately described using the Verlet-Weis corrected Percus-Yevick structure factor as input, and for a solvent penetration length equal to three percent of the excluded volume radius. This small amount of solvent permeability of the microgel particles has a significant dynamic effect at larger concentrations.

1 Introduction

Suspensions of globular colloidal particles with internal hydrodynamic structure, and different surface boundary conditions, are abundant in soft matter science. Examples of technological and biomedical relevance are non-ionic and ionic microgel particles, and core-shell particles consisting of a dry spherical core and a shell of some soft material such as a polymer brush. These particulate systems are to a certain degree permeable to the solvent. Microgel particles in particular consist of a network formed by cross-linked polymer chains. They have useful features such as temperature-, pH-, salinity- and concentration-dependent¹ swelling behavior as well as elasticity and flexibility. This renders them as good candidates for various applications such as drug delivery agents^{2–4}, the engineering of tissues^{5–8}, and the modification of rheological properties⁹. The elasticity of microgels can be controlled, e.g., by the amount of crosslinker, and the length of polymer chains used in the synthetization process. Microgels can be therefore

considered as bridging the gap between genuine hard spheres and ultra-soft colloids¹⁰.

Although microgel and core-shell particle systems have been intensely studied experimentally over the past years, a quantitative theoretical description of the diffusion and rheological properties of concentrated suspensions is still in demand. This is owed to the complicated many-particle hydrodynamic interactions (HIs) which are significantly influenced by the hydrodynamic structure of the particles. A theoretical understanding of the influence of HIs on colloidal transport properties such as translational and rotational diffusion coefficients, the generalized sedimentation coefficient (hydrodynamic function), and high-frequency and zero-frequency viscosities is of key importance also in process engineering, e.g. in filtration and fractionation processes^{11,12}, and for the energy cost reduction in the transportation of colloidal suspensions through viscosity minimization.

On a coarse-grained level, the porosity-averaged fluid flow inside a solvent-permeable particle is commonly described by the Brinkman-Debye-Bueche (BDB) equation invoking the Darcy permeability, κ^2 , where $1/\kappa$ is the hydrodynamic penetration length^{13,14}. Globular particles with an on average spherically symmetric hydrodynamic structure can be characterized by a permeability coefficient, $\kappa(d)$, depending on the

^a Forschungszentrum Jülich GmbH, ICS-3 - Soft Condensed Matter, 52428 Jülich, Germany

^b Institute of Physical Chemistry, RWTH Aachen University, Landoltweg 2, 52056, Aachen, Germany

* E-mail: j.riest@fz-juelich.de

radial distance, d , from the particle center¹⁵. Versatile hydrodynamic simulation tools such as the HYDROMULTIPOLE hydrodynamic force multipole method¹⁶ have been developed which allow for calculating transport properties of concentrated dispersions of hydrodynamically structured particles with the full inclusion of HIs. However, these simulations are numerically expensive, and in principle they must be performed separately for each particle model. In a recent series of papers, various short-time dynamic properties of dispersions of uniformly permeable spheres^{17–20}, and of core-shell particles with uniformly permeable shell^{21–23}, have been calculated using the HYDROMULTIPOLE method, as functions of particle concentration, reduced Darcy permeability, and shell-thickness to particle size ratio. The non-hydrodynamic direct particle interactions in these simulations have been taken for simplicity as pure hard-core interactions characterized by the excluded volume particle radius $a = \sigma/2$. Any softness in the effective pair potential, $V(r)$, between two globular particles at center-to-center distance r is hereby disregarded.

As discussed in Refs.^{22–24}, a simplifying concept allowing for abstracting from specific intraparticle structures is the so-called hydrodynamic radius model (HRM) which invokes the notion of an apparent no-slip hydrodynamic particle radius a_h (see also Refs.^{25,26}). The HRM amounts to approximating a globular particle of spherically symmetric hydrodynamic structure by a no-slip sphere of hydrodynamic radius a_h while leaving the effective pair potential unchanged. Under from an experimental viewpoint surprisingly general conditions, a_h is unequivocally determined from the measurement of a single-particle transport property such as the translational diffusion coefficient D'_0 or the intrinsic viscosity $[\eta]$. The definition of the HRM includes also spherical particles with fuzzy hydrodynamic structure and no sharp outer boundary, and with a soft pair potential such as for weakly cross-linked ionic microgels^{1,27,28}. For spherical particles having excluded volume interactions only with $a_h < a$, the HRM reduces to the so-called spherical annulus model. For the annulus model, numerically precise simulation results for various short-time dynamic properties have been given in Ref.²¹. The good accuracy of the simplifying HRM was demonstrated in Refs.^{19,21,29} for uniformly permeable and core-shell spheres with pure excluded volume interactions, by a thorough comparison with simulation results. While a single hydrodynamic radius suffices to characterize the hydrodynamic intraparticle structure of many experimentally realized suspensions, regarding its influence on configuration-averaged transport properties, the replacement of the soft pair potential by an effective hard-core potential is in general a less successful strategy. Methods of calculating static suspension properties based on an effective hard-sphere potential such as the Barker-Henderson perturbation scheme, a second virial coefficient mapping, and additional variational methods commonly fail if the longer-ranged, soft

part of the pair potential stretches out significantly beyond the physical excluded volume radius. For charge-stabilized colloids, e.g., this has been shown in Refs.^{30,31}.

In this article, we present an easy-to-apply set of analytic methods, referred to for short as a toolbox, to calculate short-time transport properties of concentrated dispersions consisting of spherical colloidal particles with internal hydrodynamic structure, and with direct interactions given by the hard-core and two-parameter soft Hertz potentials. The latter potential is continuous and bounded, and it describes the energy penalty caused by the elastic deformation of two colliding spheres^{27,32}. The Hertz potential has been shown to be a useful description of the direct interactions between non-ionic, soft microgels of low cross-link density, and this even though the particles are of a distinctly inhomogeneous structure^{27,33}. Our toolbox is based on the HRM, and it takes advantage of the tabulated simulation data for spherical annulus particles listed in Ref.²¹. The toolbox incorporates in particular useful approximate scaling relations for the wavenumber-dependent sedimentation coefficient, $H(q)$, the short-time self-diffusion coefficient D_S , and the high-frequency viscosity η_∞ . These quantities are routinely determined in dynamic scattering experiments. The scaling relation expressions are known for permeable particles with hard-core interactions to be in remarkably good agreement with simulation data^{17,18,34}. We show that they apply likewise to particles with a soft pair potential, and we augment them by scaling expressions for the collective diffusion coefficient, D_C , and the associated sedimentation coefficient K .

Moreover, we extend the toolbox to long-time dynamic properties of concentrated systems of hydrodynamically structured particles, including the low-shear zero-frequency suspension viscosity η , and the long-time translational self-diffusion coefficient D_L . Different from their short-time siblings, long-time transport properties are affected additionally by the non-instantaneous microstructural relaxation of the cloud of neighboring Brownian particles. This relaxation is controlled both by direct and hydrodynamic interactions. The toolbox extension to long-time properties combines the HRM with a factorization approximation method introduced originally by Medina-Noyola³⁵, and elaborated subsequently by Brady^{36,37} and Banchio *et al.*³⁸. The HRM is useful also for long-time properties, since the hydrodynamic mobilities in the generalized many-particle Smoluchowski diffusion equation describing the configurational distribution function are time-independent³¹.

We demonstrate the accuracy of our user-friendly toolbox through the analysis of a light scattering study on a concentration series of non-ionic, submicron-sized PNIPAM microgel particles dispersed in dimethylformamide (DMF). We show that the static and dynamic scattering data for the static structure factor $S(q)$ and hydrodynamic function $H(q)$, respec-

tively, can be quantitatively described in the complete experimental wavenumber range, on using a deduced solvent penetration length equal to three percent of the particle diameter. Calculations based on the Hertz potential show that the PNIPAM microgels behave statically as effective hard spheres in the whole fluid-phase concentration regime.

The paper is organized as follows: The structure factor and the associated radial distribution function (RDF), $g(r)$, of the Hertz potential model are discussed in Subsec. 2.1, and compared with static light scattering data of non-ionic PNIPAM microgels. Subsec. 2.2 describes how hydrodynamic particle structures are related to the generic HRM, exemplified for the two important examples of uniformly permeable spheres and non-permeable rigid spheres with partial hydrodynamic surface slip. Sec. 3 includes the discussion of various short-time dynamic properties, including $H(q)$, D_S , K , and the high-frequency viscosity η_∞ . Approximate analytic expressions for these quantities are presented, and the accuracy of these expressions is scrutinized against simulation results for the spherical annulus model. In Sec. 4, the toolbox results are compared with static and dynamic light scattering (SLS and DLS) data by Eckert *et al.* on PNIPAM microgel suspensions. Sec. 5 describes the extension of the toolbox to long-time transport properties including the long-time translational self-diffusion coefficient D_L and the zero-frequency viscosity η . Our conclusions are contained in Sec. 6. The pairwise additivity (PA) and the self-part corrected Beenakker Mazur methods of calculating short-time transport properties are explained in the Appendices A and B, respectively, in the context of the HRM.

2 Equilibrium Microstructure and Hydrodynamic Radius Model

2.1 Static pair correlations

Owing to the many possible applications, various theoretical schemes have been developed for the analytic calculation of static properties of microgel suspensions. Progress in this direction was made, in particular for ionic microgels, through the development of effective pair potentials characterized by the suspension temperature and salinity, and the bare charge of the microgel particles^{39–41}. The validity of these effective pair potentials has been scrutinized in various joint theoretical-experimental studies (see e.g. Refs.^{27,42}). In contrast to ionic microgels, the effective pair potentials used for non-ionic soft microgels where short-range interactions are not masked by the longer-ranged electrostatic repulsion are to date still on a more heuristic level. The pronounced dependence of the pair potential in non-ionic microgel systems on ambient and intra-particle conditions such as the solvent quality and temperature, number and distribution of crosslinker, and length and

functionality of polymer chains requires a larger number of parameters characterizing the effective pair potential on a microscopic level. On a more coarse-grained level, simplifying pair potentials have been used such as the hard-sphere⁴³ and elastic Hertz^{27,33} potentials, and certain ultra-soft pair potentials¹⁰. The intricate dependence on environmental parameters is hidden in these coarse-grained potentials in a reduced number of interaction parameters such as the effective interaction strength and the effective particle radius.

A useful coarse-grained effective pair potential for non-ionic globular microgel particles is the Hertz potential,

$$\beta V(r) = \begin{cases} \varepsilon \left(1 - \frac{r}{\sigma_s}\right)^{\frac{5}{2}} & r \leq \sigma_s \\ 0 & r > \sigma_s, \end{cases} \quad (1)$$

which describes the elastic deformation of two spheres in contact. Here, $\beta = 1/(k_B T)$ is the reduced inverse temperature with Boltzmann constant k_B and absolute temperature T , and σ_s plays the role of an effective soft particle diameter. For distances $r \geq \sigma_s$, two Hertz model particles do not interact with each other. The strength of the continuous potential is quantified by the non-dimensional elasticity parameter (effective potential strength),

$$\varepsilon = \frac{2Y\sigma_s^3}{15k_B T(1-\nu^2)}, \quad (2)$$

depending on the bulk modulus Y and the Poisson ratio ν of a particle^{27,32}. On approximating the mesoscopic particle elastic moduli Y and ν by macroscopic values, the estimate $\varepsilon \approx 10^4 \sim 10^5$ is obtained for micron-sized microgels. Note here the strong size dependence $\varepsilon \propto \sigma_s^3$, implying a significantly decreased potential strength for smaller microgel particles. While our work is concerned with the fluid-like concentration regime only, as an aside we remark that quite different solid phases are observed in concentrated Hertz potential systems for different values of ε ⁴⁴. The Hertz potential has been shown to provide a nearly fit-parameter free description of the structure and phase behavior of neutral microgel systems, in good agreement with experimental results for various particle sizes^{27,33}, and values of ε in the range from $10^2 - 10^4$. While for large ε the Hertz and hard-sphere potentials lead to very similar results for the equilibrium microstructure, the effective diameter in the Hertz potential is in general somewhat larger than the corresponding hard-sphere value, i.e. $\sigma_s \gtrsim \sigma$. This reflects the fact that the Hertz potential incorporates overall the softness of a microgel particle which in turn originates from the radially inhomogeneous crosslinker density.

For very large values of ε , the Hertz potential is practically indistinguishable from the hard-sphere potential

$$V_{\text{HS}}(r) = \begin{cases} \infty & r \leq \sigma = 2a \\ 0 & r > \sigma, \end{cases} \quad (3)$$

with σ_s playing now the role of the hard-sphere diameter σ . Considering the high-energy deformation penalty ε of micron-sized, non-ionic PNiPAM microgels, the usage of the hard-sphere potential in place of the Hertz potential is well justified (see inset in Fig. 3). This is advantageous from a theoretical viewpoint since colloidal hard spheres are among the most thoroughly studied soft matter systems.

In addition to being the key quantities in static scattering experiments on concentrated suspensions, the static structure factor, $S(q)$, and its associated RDF, $g(r)$, are required as inputs in various methods of calculating colloidal transport properties. For the Hertz potential model, we determine the two pair correlation functions numerically from solving the approximate Percus-Yevick (PY) integral equation^{45,46}. The corresponding pair correlation functions for the hard-sphere model are determined from the analytic PY solution combined with the Verlet-Weis (VW) correction⁴⁷ incorporating the accurate Carnahan-Starling equation of state (see also Ref.⁴⁸). The VW correction compensates in particular the overestimation by the PY solution of the principal peak height, $S(q_m)$, of the hard-sphere structure factor for volume fractions $\phi = (\pi/6)n\sigma^3 \gtrsim 0.4$. Here, n is the number concentration of particles.

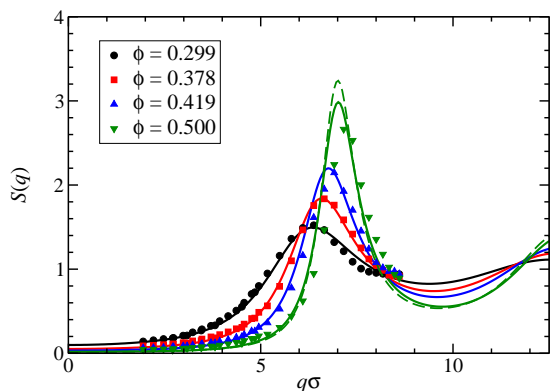


Fig. 1 Comparison of the experimental static structure factor, $S(q)$, of PNiPAM microgels (filled symbols, taken from Ref.⁴³) with the Verlet-Weis corrected Percus Yevick prediction (solid lines), for various particle volume fractions ϕ as indicated. The bare PY structure factor for the largest considered volume fraction $\phi = 0.5$ is represented by the dashed curve.

In Fig. 1, we compare the PY-VW structure factors for the hard-sphere model with static light scattering results by Eckert and Richtering⁴³ for a concentration series of non-ionic poly(N-isopropylacrylamide) (PNiPAM) microgels in DMF. The details of the particle synthesis are given in Refs.^{43,49,50}. In our PY-VW calculations, we have used the experimen-

tally obtained (mean) particle diameter $\sigma = 240$ nm, and the (volume-swelling corrected) volume fractions ϕ as given in Ref.⁴³. We refer to this reference for the details on how the volume fractions have been determined. The agreement between the experimental and PY-VW structure factors is good even for small wavenumbers q . There is in particular a significantly improved agreement for the largest considered volume fraction (dashed curve in Fig. 1), as compared to the bare PY $S(q)$ used in the earlier work⁴³. The remaining small deviations for the most concentrated system at $\phi = 0.5$ can be at least partially attributed to experimental uncertainties, and possibly also to the breakdown of the exact factorization of the mean scattered intensity into static structure and form factors as discussed by Likos *et al.*^{51,52}. In Fig.

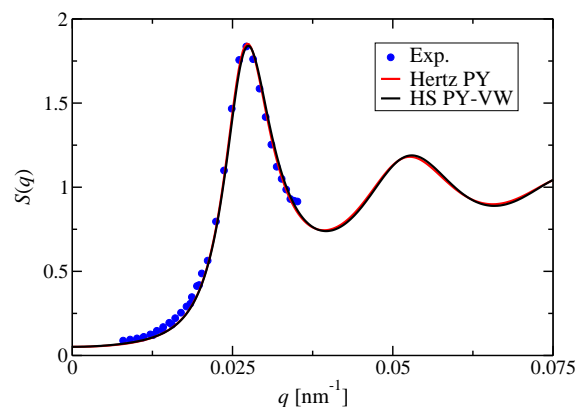


Fig. 2 Experimental structure factor at $\phi = 0.378$ (filled circles) in comparison with the best-fit hard-sphere model PY-VW $S(q)$ (black solid line), and the best-fit Hertz model $S(q)$ calculated in PY approximation (red solid line). For the Hertz model, the parameters $\varepsilon = 10^4$, $\sigma_s = 245$ nm, and $\phi_s = 0.398$ have been used.

2, the experimental structure factor of PNiPAM microgels is compared, for $\phi = 0.378$, with the best-fit hard-sphere and the best-fit Hertz potential structure factors. For the Hertz model system, the parameter values $\sigma_s = 245$ nm, $\varepsilon = 10^4$, and $\phi_s = (\pi/6)n\sigma_s^3 = 0.398$ have been used. The theoretical curves coincide practically, as expected for the invoked large value of ε which restricts the softness range of the Hertz potential to a narrow interval around the effective diameter σ_s . This can be noticed from the inset of Fig. 3. The remnant potential softness still necessitates a slightly larger effective diameter σ_s than the hard-sphere model value $\sigma = 240$ nm, for the Hertz potential incorporates the interactions by dangling polymer chains at the periphery of microgel particles. The larger particle size in the Hertz potential model goes along with a larger volume fraction ϕ_s than that used in the best-fit hard-sphere model result. With increasing volume fraction in

the range $\phi_s \in [0.299 - 0.5]$, a slight decrease of the best-fit effective diameter σ_s is observed. However, owing to the smallness of the particle size shrinkage, for the considered PNiPAM in DMF system this effect can be disregarded in its influence on static and dynamic properties.

The $g(r)$'s corresponding to the best-fit Hertz and hard-sphere

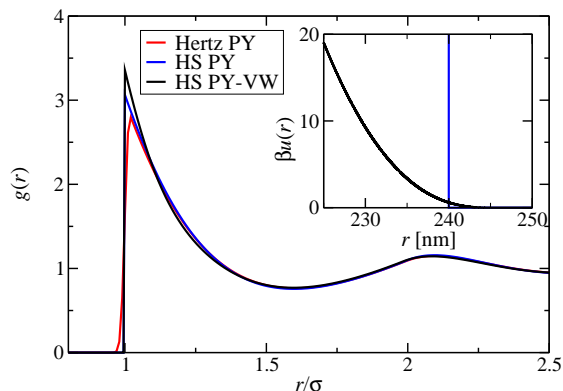


Fig. 3 Radial distribution functions, $g(r)$, corresponding to the hard-sphere and Hertz potential structure factors in Fig. 2. The inset compares the hard-sphere and Hertz pair potential, for the parameters in Fig. 2.

model structure factors in Fig. 2 are depicted in Fig. 3. The slight softness of the Hertz potential is reflected in the somewhat reduced peak height of $g(r)$ (red solid curve), and in the slight extension of the RDF into the overlap region $r < \sigma_s$. From Figs. 2 and 3, we conclude that the pair correlations of the considered PNiPAM suspensions in the experimental concentration range are fully compatible with the simple hard-sphere potential. For microgels of lower crosslinker density and smaller size where the softness of the particles is important, the Hertz potential model should be used.

2.2 Hydrodynamic Particle Modeling

As an illustration of the concept of a hydrodynamic radius a_h and its associated slip length L_h , consider two simple hydrodynamic particle models, namely uniformly fluid-permeable rigid spheres^{53,54}, and non-permeable rigid spheres with Navier partial slip hydrodynamic surface boundary condition⁵⁵. The physical (material) sphere radius in both models is denoted here by a .

In the uniformly-permeable sphere model, the pore-size averaged fluid flow inside a particle is described by the Brinkman-Debye-Bueche (BDB) equation, and the outside flow by the low-Reynolds-number Stokes equation⁵⁶. The imposed boundary condition is here that the fluid velocity and

tangential stress are continuous across the particle surface. The suspension transport properties in this model depend on the material-specific parameter

$$\lambda_\kappa = \frac{1}{\kappa a}, \quad (4)$$

equal to the ratio of the hydrodynamic penetration length, $1/\kappa$, and particle radius a . The penetration length is roughly equal to the mean pore size of the rigid skeleton of a permeable sphere. In the limit $\lambda_\kappa \rightarrow 0$ of vanishing mean pore size, a non-permeable sphere with no-slip hydrodynamic boundary condition (BC) on its surface is obtained. For the BDB equation to apply, the mean pore size should be no larger than one tenth of the particle radius so that $\lambda_\kappa \leq 0.1$. The present model has been generalized to spherical particles with a permeability profile $\kappa(r)$ varying with the radial distance (see, e.g. Ref.⁵³) such as core-shell particles^{21,57-59} consisting of a dry core and a permeable outer shell. The core-shell model describes in a coarse-grained manner the hydrodynamic effect, e.g., of a polymer brush surrounding the core.

The Navier partial-slip model on the other hand describes fluid-impermeable colloidal spheres where the fluid is allowed to partially slip along their surfaces. The associated Navier partial-slip BC demands for a stationary sphere at each surface point the proportionality of surface-tangential fluid velocity, \mathbf{u}_\parallel , and shear-stress, \mathbf{t}_\parallel , according to

$$\mathbf{u}_\parallel = \frac{l_s}{\eta_0} \mathbf{t}_\parallel. \quad (5)$$

The proportionality constant is given by the ratio of the so-called Navier length, l_s , and the fluid shear viscosity η_0 . In the limit $l_s^* \rightarrow 0$, the no-slip BC describing zero surface slip is recovered. Here, $l_s^* = l_s/a$ is the reduced Navier length. In the opposite limit $l_s^* \rightarrow \infty$, the free-surface BC of zero tangential stress is obtained, corresponding to fluid perfectly slipping along the sphere surface in form of local plug flow. The Navier partial-slip BC can serve as an effective description of a hydrophobic particle surface, and of a rigid particle with surface roughness and corrugations⁶⁰. It is also applicable when non-adsorbing (short) polymers are dispersed in the fluid, owing to the formation of a thin clear-fluid depletion layer at the particle surfaces⁶¹.

The hydrodynamic radius is a single-particle property which depends on the intra-particle hydrodynamic structure of the spherical particle, and in principle also on the considered single-particle transport property. It can be defined operationally through the Stokes-Einstein-Debye expressions

$$D_0^i(\alpha) = \frac{k_B T}{6\pi\eta_0 a_h^i(\alpha)} \quad (6)$$

$$D_0^r(\alpha) = \frac{k_B T}{8\pi\eta_0 a_h^r(\alpha)^3}, \quad (7)$$

for the translational and rotational diffusion coefficients D_0^t and D_0^r , respectively, of an isolated spherical particle in an infinite fluid. An additional definition not considered here is based on the intrinsic viscosity, $[\eta]$, of dispersed spheres¹⁹. Here, α denotes a set of parameters characterizing the hydrodynamic particle red structure. For the two considered models is $\alpha = \{\lambda_x, l_s^*\}$. The respective translational and rotational hydrodynamic radii are^{53,54}

$$\frac{a_h^t(\lambda_x)}{a} = \frac{2x^2(x - \tanh(x))}{2x^3 + 3(x - \tanh(x))} \quad (8)$$

$$\frac{a_h^r(\lambda_x)}{a} = \left[1 + \frac{3}{x^2} - \frac{3 \coth(x)}{x} \right]^{\frac{1}{3}}, \quad (9)$$

for a homogeneously permeable sphere with $x = 1/\lambda_x$, and⁵⁵

$$\frac{a_h^t(l_s^*)}{a} = \frac{1 + 2l_s^*}{1 + 3l_s^*} \quad (10)$$

$$\frac{a_h^r(l_s^*)}{a} = \left(\frac{1}{1 + 3l_s^*} \right)^{1/3}, \quad (11)$$

for a Navier partial-slip sphere.

One can associate each hydrodynamic radius a_h with a reduced hydrodynamic slip length, L_h^* , through

$$L_h^*(\alpha) = \frac{L_h(\alpha)}{a} = 1 - \frac{a_h(\alpha)}{a}. \quad (12)$$

The quantity L_h^* is the relative radial distance, $L_h = a - a_h$, of the apparent no-slip spherical surface inside the particle to its outside surface, in units of the outside surface radius a . Except for λ_x , the asterisk is used throughout to label lengths given in units of a .

In the experimentally common situation where L_h^* is small, curvature effects are negligible and the particle-fluid interface can be described as flat. As it is explained in Ref.²³, the key point to notice is that the reduced slip length, $L_{h,f}^* = 1 - a_{h,f}/a$, in the flat-interface approximation and its associated flat-interface hydrodynamic radius, $a_{h,f}$, are independent of the single-particle transport properties D_0^t , D_0^r and $[\eta]$ used in their definition. Since each of these transport properties is associated with a particular ambient velocity field, e.g. with a constant flow field in case of D_0^t , an equivalent statement is that $L_{h,f}$ is independent of the ambient flow.

It was shown in Ref.²³ that the relations

$$L_h^*(\alpha) = L_{h,f}^*(\alpha) [1 + \mathcal{O}(L_{h,f}^*(\alpha))] \quad (13)$$

$$a_h^*(\alpha) = a_{h,f}^*(\alpha) [1 + \mathcal{O}(L_{h,f}^*(\alpha)^2)], \quad (14)$$

apply universally to rigid spheres with arbitrary, non-singular spherically symmetric hydrodynamic structures and boundary conditions, independent of the invoked single-particle transport property.

These relations are readily verified, using Eqs. (8) - (11), for the special case of a Navier partial-slip sphere where the flat-interface slip length is equal to

$$L_{h,f}^*(l_s^*) = l_s^*, \quad (15)$$

and for a uniformly permeable sphere where

$$L_{h,f}^*(\lambda_x) = \lambda_x. \quad (16)$$

Note that the slip length L_h is equal to the Navier length l_s in the flat-interface limit only.

Eqs. (13-14) do not apply to non-rigid particles such as spherical liquid droplets, and rigid particles of singular hydrodynamic structure. The latter case is exemplified in Ref.⁵⁴ by a hollow sphere with a uniformly permeable rigid shell of infinitesimal thickness. The hydrodynamic radii a_h^t and a_h^r of the ultra-thin hollow sphere differ already to linear order in the smallness parameter λ_x . As for a droplet, an inscribed apparent no-slip spherical surface which is necessarily rigid can not be introduced for the singular hollow-sphere example.

Eqs. (8-11) can be inverted to obtain the material-specific parameters λ_x and l_s^* in terms of the ratio

$$\gamma = \frac{a_h}{a}, \quad (17)$$

or likewise in terms of the reduced width (slip length), $\bar{\gamma} = 1 - \gamma$, of the apparent fluid annulus region surrounding the apparent no-slip sphere. The parameter γ completely characterizes the intra-particle hydrodynamic structure in the hydrodynamic radius model (HRM) where spherical particles of arbitrary hydrodynamic structure are described hydrodynamically as no-slip spheres of reduced radius a_h , for unchanged pair potential. This implies in particular an unchanged excluded volume radius $a > a_h$.

Numerical results illustrating this inversion are depicted in Fig. 4 where the reduced penetration length of a permeable sphere, $\lambda_x^{t,r}$, and the reduced slip length of a Navier partial-slip sphere, $(l_s^*)^{t,r}$, are plotted as functions of $\bar{\gamma}$. The reduced lengths derived from the translational (rotational) Stokes-Einstein-(Debye) relation are labeled by the superscript t (superscript r). For a thin annulus shell with $\gamma > 0.9$, the four reduced lengths are small and commonly described by the dashed-dotted line $\bar{\gamma}$, corresponding to $\lambda_x \approx L_h$ and $l_s^* \approx L_h$. This situation is common to colloidal systems for which values $\lambda_x < 0.05$ are typically found, and for which the Navier length is commonly equal to a few nanometers.

Differences between the considered lengths are significant for larger values of $\bar{\gamma}$. For a given reduced hydrodynamic radius $\gamma = a_h/a$, two different values $\lambda_x^t \neq \lambda_x^r$ are then obtained. The perfect-slip limit $l_s^* \rightarrow \infty$ corresponds to $\bar{\gamma} = 1/3$ for translational, and to $\bar{\gamma} = 1$ for rotational diffusion. While a rotating perfect-slip sphere experiences no friction, akin to a point particle for which $\gamma = 0$, the values of $\bar{\gamma}$ for a translating Navier

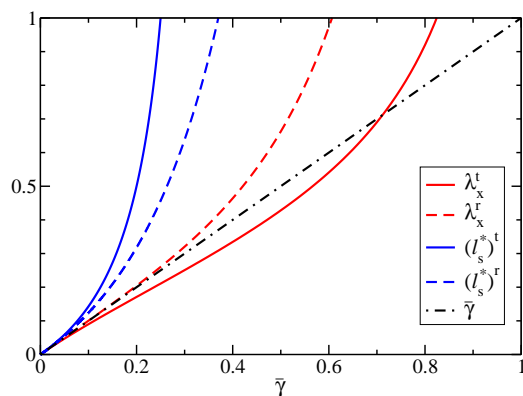


Fig. 4 Reduced fluid penetration length $\lambda_x^{t,r}$ (red lines) and reduced Navier length $(l_s^*)^{t,r}$ (blue lines), as functions of the reduced fluid annulus width $\bar{\gamma} = 1 - \gamma$. Solid lines (dashed lines) describe quantities derived from the translational (rotational) single-sphere Stokes-Einstein-(Debye) relation.

sphere do not exceed $1/3$. Regarding the translational diffusion coefficient, a perfect-slip sphere with $\gamma = 2/3$ has the same value, $D_0^t = k_B T / (4\pi\eta_0 a)$, as a uniformly permeable sphere with $\lambda_x \approx 0.278$. However, such a large value of λ_x is unrealistic. In order for the BDB equation to describe flow inside a permeable particle, λ_x should be no larger than 0.1 , corresponding to a maximally allowed penetration length equal to one-tenth of the particle radius.

3 Short-time Transport Properties

In studying the dynamics in dispersions of colloidal particles, one distinguishes the short-time regime where $\tau_B \ll t \ll \tau_D$ from the long-time regime where $t \gg \tau_D$. Here, t denotes the correlation time of particle concentration fluctuations, and τ_B and τ_D are the characteristic particle momentum relaxation and diffusion times, respectively. The time τ_B is the decay time of velocity correlations of a particle. For sub-micron sized particles in a low-viscosity fluid such as the here considered PNIPAM in DMF microgels, τ_B is of the order of microseconds. The particle diffusion time can be estimated by $\tau_D \sim a^2/D_0^t$ which for the considered microgels is in the millisecond range. In the short-time regime, the particle configuration has changed so little that the slowing influence of non-hydrodynamic direct interactions is not yet operative, different from the solvent-mediated HIs which act quasi-instantaneously on the colloidal scale. Short-time transport properties are thus expressible as simple equilibrium averages, with the direct interactions entering only by their influ-

ence on the equilibrium microstructure, e.g. on the RDF $g(r)$. Long-time transport properties are additionally influenced by the Brownian motion of the particles so that they depend in a direct way both on direct and hydrodynamic interactions.

In this section, we describe our analytic toolbox of calculating short-time diffusion and rheological properties of hydrodynamically structured particles, in the framework of the HRM. In the subsequent sections, the toolbox is used for analyzing light scattering data on PNIPAM in DMF suspensions.

3.1 Hydrodynamic function

The colloidal short-time regime is probed in DLS experiments by analyzing the initially exponential decay,

$$S(q, t \ll \tau_D) = S(q) \exp[-q^2 D(q)t], \quad (18)$$

of the dynamic structure factor, $S(q, t)$, in its dependence on the modulus q of the single-scattering wave vector \mathbf{q} . The dynamic structure factor is the q -th Fourier component of spatio-temporal correlations in thermally induced particle concentration fluctuations. On basis of the many-particle generalized Smoluchowski equation (GSME), the wavenumber-dependent diffusion function, $D(q)$, quantifying the short-time exponential decay can be expressed by the ratio⁴²

$$D(q) = D_0^t \frac{H(q)}{S(q)}, \quad (19)$$

of the hydrodynamic function $H(q)$ and the static structure factor $S(q)$. The hydrodynamic function is the key quantity containing information on colloidal short-time diffusion processes. It can be expressed by the equilibrium configurational average³¹,

$$H(q) = \left\langle \frac{k_B T}{N D_0^t} \sum_{i,j=1}^N \hat{\mathbf{q}} \cdot \boldsymbol{\mu}_{ij}(\mathbf{X}) \cdot \hat{\mathbf{q}} e^{i\mathbf{q} \cdot [\mathbf{R}_i - \mathbf{R}_j]} \right\rangle, \quad (20)$$

over an ensemble of N colloidal spheres, with the thermodynamic limit $N \rightarrow \infty$ for a fixed particle concentration n performed subsequently, in order to describe a macroscopically large scattering volume. Here, $\hat{\mathbf{q}}$ is the unit vector in the direction of \mathbf{q} , and $k_B T$ is the system temperature T multiplied by the Boltzmann constant. The translational mobility tensor $\boldsymbol{\mu}_{ij}$ linearly relates the hydrodynamic force acting on particle j at the instant position \mathbf{R}_j to the resulting velocity change of a particle i . It depends on the hydrodynamic structure of the globular particles, e.g. on particle sizes, surface BCs and fluid permeability, and on the many-particles HIs for an instant configuration, $\mathbf{X} = \{\mathbf{R}_1, \dots, \mathbf{R}_N\}$, of particle centers.

Without HIs, $H(q)$ would be identically equal to one independent of q . Any wavenumber dependence reflects thus the

presence of HIs. The hydrodynamic function consists of a q -independent self-part and a distinct part, i.e.

$$H(q) = \frac{D_S}{D'_0} + H_d(q), \quad (21)$$

with the distinct part, $H_d(q)$, approaching its asymptotic value zero for $q \rightarrow \infty$. Thus, for large q corresponding to small distances resolved, $H(q)$ reduces to the short-time self-diffusion coefficient, D_S , expressed in units of the single-sphere translational diffusion coefficient D'_0 . The coefficient D_S quantifies the initial (i.e., short-time) slope of the mean-squared displacement of a particle in presence of other ones. Owing to the slowing influence of the HIs at non-zero particle concentrations, D_S is smaller than D'_0 to which it reduces at infinite dilution only.

The hydrodynamic function has the physical interpretation of a short-time generalized sedimentation coefficient for a homogeneous suspension of monodisperse colloidal spheres subjected to a weak force field colinear with \mathbf{q} and oscillating spatially as $\cos(\mathbf{q} \cdot \mathbf{r})$ with positions \mathbf{r} ⁶². For $q \rightarrow 0$, a homogeneous force field is recovered such as the local gravitational field on earth. Consequently,

$$K = \frac{V_{\text{sed}}}{V_0} = \lim_{q \rightarrow 0} H(q) \quad (22)$$

is the short-time average sedimentation velocity, V_{sed} , of hydrodynamically interacting colloidal particles, normalized by the particle model dependent mean velocity, V_0 , of an isolated particle sedimenting in the same force field. The sedimentation coefficient K is related to the short-time collective diffusion coefficient, D_C , by

$$D_C = D'_0 \frac{K}{S(0)}, \quad (23)$$

where for monodisperse particles $S(0) \equiv \lim_{q \rightarrow 0} S(q)$ is the relative osmotic compressibility of the suspension. At larger concentrations where $S(0)$ is small, D_C is significantly larger than D'_0 . In principle, the short-time coefficient D_C should be distinguished from the associated long-time collective diffusion coefficient appearing in Fick's law of macroscopic gradient diffusion. The latter, however, is only slightly smaller than the short-time coefficient, by less than 7% even for a concentrated suspension of no-slip colloidal hard spheres at volume fraction $\phi = 0.45$ ⁶³. The difference between the two collective diffusion coefficients can be expected to be even smaller for particles with weaker HIs such as permeable and partial-slip spheres, and charge-stabilized particles with long-range electrostatic repulsion. Different from collective diffusion and sedimentation, the long-time translational self-diffusion coefficient D_L can be substantially smaller than its short-time sibling D_S , owing to the retarding relaxation of

next-neighbor particle cages which are slightly distorted from their equilibrium spherical symmetry at long times. For colloidal hard spheres at the freezing transition concentration, e.g., $D_L/D_S \approx 0.1$ according to the empirical freezing rule by Löwen *et al.*^{64,65}.

In this work, we discuss useful analytic scaling relations for the calculation of short-time diffusion and viscosity properties of suspensions of internally structured particles. These relations are complemented by two semi-analytic and easy-to-implement approximation schemes which have been successfully applied in the past to suspensions of no-slip neutral and charge-stabilized spherical particles^{42,66–68}. The first scheme is the so-called pairwise-additivity (PA) approximation where all two-body contributions to the hydrodynamic mobilities $\boldsymbol{\mu}_{ij}$ are accounted for including near-contact lubrication terms, but three-body and higher-order contributions are disregarded. The PA method is thus well suited for low concentrations where it is basically exact. The second method is a self-part corrected improved version⁴² of the $\delta\gamma$ renormalized concentration fluctuation expansion by Beenakker and Mazur^{69–71}, where many-particle HIs contributions are approximately accounted for in terms of so-called ring diagrams, but with lubrication corrections disregarded (see also Ref.⁷²). The $\delta\gamma$ method is well suited in particular for larger concentrations. The only input required by these methods is the RDF or likewise the static structure factor. The explicit expressions by both methods for $H(q)$ and the high-frequency (short-time) suspension viscosity η_∞ , generalized to the HRM, are presented in the Appendices A and B, respectively.

A key observation regarding the translational mobility tensors $\boldsymbol{\mu}_{ij}$ of hydrodynamically structured spherical particles is the relation

$$\boldsymbol{\mu}_{ij}(\mathbf{X}) = \boldsymbol{\mu}_{ij;\text{HRM}}(\mathbf{X}; a_{h,f}) \left[1 + \mathcal{O}(L_{h,f}^{*2}) \right], \quad (24)$$

where $\boldsymbol{\mu}_{ij;\text{HRM}}(\mathbf{X}; a_{h,f})$ are the mobility tensors of the associated HRM. The relation follows from Eqs. (13) and (14) in conjunction with a general scattering series expansion of the exact N -sphere translational mobility tensors^{22,23}. Since the short-time transport properties are equilibrium averages of specific mobility tensor elements, it follows that

$$H(q) = H_{\text{HRM}}(q) \left[1 + \mathcal{O}(L_{h,f}^{*2}) \right] \quad (25)$$

with an analogous expression valid for η_∞ . Thus, the error introduced in calculating short-time transport properties of hydrodynamically structured particles using the simplifying HRM is of $\mathcal{O}(L_{h,f}^{*2})$ small.

3.2 Translational self-diffusion

In Refs.^{34,42}, it was shown by comparison with computer simulation results for uniformly permeable hard spheres with

$\lambda_x < 0.2$ that D_S normalized by its infinite dilution D'_0 is well represented by the simple scaling relation,

$$\frac{D_S(\phi, \lambda_t)}{D'_0(\lambda_t)} = 1 + \lambda_t \phi (1 + 0.12\phi - 0.70\phi^2), \quad (26)$$

for all $\phi \leq 0.5$ and with an accuracy of 3.5% or better. A similar scaling relation has been obtained for the short-time rotational self-diffusion coefficient of permeable-sphere suspensions with hard-core interactions³⁴. The only dependence in Eq. (26) on the permeability parameter λ_x characterizing the intra-particle hydrodynamic structure is contained in the second virial coefficient, $\lambda_t = \lambda_t(\lambda_x)$, which is the linear coefficient in the expansion of D_S in powers of ϕ . Eq. (26) states that the D_S for hydrodynamically structured particles can be scaled to the corresponding coefficient of no-slip hard spheres where $\lambda_x = 0$ and $\lambda_t(\lambda_x = 0) = -1.8315$.

In fact, on the level of the HRM model Eq. (26) is applicable to suspensions of hard spheres of arbitrary hydrodynamic structure, with deviations from the D_S of the actual particle system being of quadratic order small in the reduced slip length L_h^* according to Eq. (25). On recalling that for spherical particles with hard-core direct interactions only the HRM reduces to the spherical annulus model, the only input required in Eq. (26) is the second virial coefficient, $\lambda_t(\gamma)$, of spherical annulus particles depending on the ratio, $\gamma = a_h/a$, of hydrodynamic and hard-core radius. Using for $\lambda_t(\gamma)$ the Eq. (63) in Appendix A in conjunction with tabulated numerical values for the longitudinal and transversal mobility coefficients, $x_{11}(r)$ and $y_{11}(r)$, of two no-slip spheres of radius a_h calculated using the method of Jeffrey and Onishi⁷³, we have obtained numerically precise values for the second virial coefficient of spherical annulus particles. These values are described to high accuracy by the polynomial fit

$$\lambda_t(\gamma) = -1.8315 + 7.820\bar{\gamma} - 14.231\bar{\gamma}^2 + 14.908\bar{\gamma}^3 - 9.383\bar{\gamma}^4 + 2.717\bar{\gamma}^5, \quad (27)$$

accounting for the numerically correct limiting value $\lambda_t(\gamma = 1) = -1.8315$ of no-slip hard spheres.

In Fig. 5, the high accuracy of the polynomial fit in Eq. (27) is shown in comparison with earlier numerical results^{22,74} for the second virial coefficient of spherical annulus particles. Note that $\lambda_t(\gamma = 0) = 0$ relates to the limiting case of spherical annulus particles interacting hydrodynamically as point particles for which there are no hydrodynamic self-reflections so that D_S reduces to D'_0 independent of ϕ . The associated long-time coefficient D_L for $\gamma = 0$ is still ϕ -dependent and smaller than D'_0 .

The accuracy of the analytic scaling formula in Eq. (26) in combination with Eq. (27) for the short-time self-diffusion coefficient of spherical annulus particle systems is established in

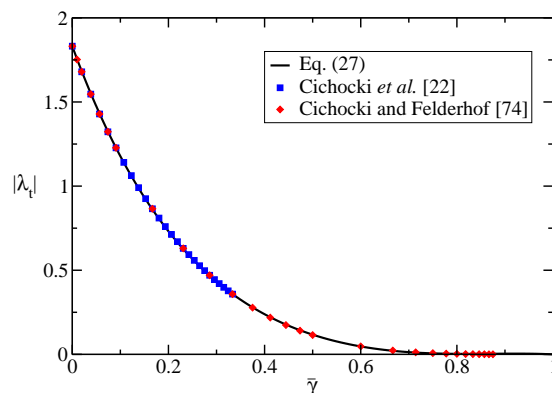


Fig. 5 Modulus $|\lambda_t|$ of the first-order virial coefficient of D_S in the spherical annulus model, as a function of the reduced fluid annulus shell width $\bar{\gamma} = 1 - \gamma$. Solid line: Polynomial fit according to Eq. (27). Filled squares: Tabulated values by Cichocki *et al.*²² for spherical annulus particles with $\bar{\gamma} \leq 1/3$. Filled diamonds: Tabulated values by Cichocki and Felderhof⁷⁴.

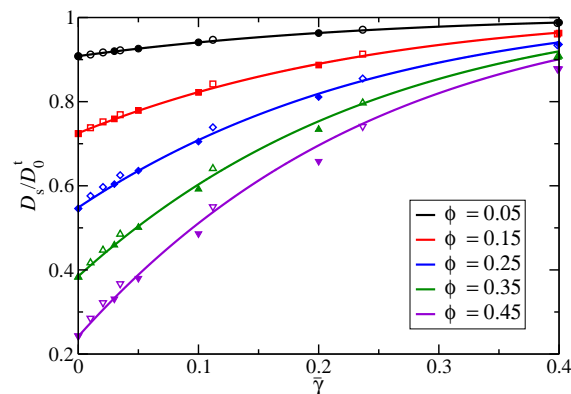


Fig. 6 Results for the reduced self-diffusion coefficient, D_S/D'_0 , of the spherical annulus model as function of $\bar{\gamma} = 1 - \gamma$, for several volume fractions ϕ as indicated. Solid lines: Prediction by the scaling formula in Eq. (26) in combination with the first order virial coefficient fitting polynomial in Eq. (27). Closed symbols: HYDROMULTIPOLE simulation data for the spherical annulus model tabulated in Ref.²¹. Open symbols: Simulation data for uniformly permeable spheres tabulated in Ref.¹⁷, with Eq. (8) used in mapping the permeability parameter λ_x onto the annulus model parameter $\gamma = a_h/a$ (recall Fig. 4).

Fig. 6 by the comparison with high-precision benchmark simulation data for the spherical annulus²¹ and uniformly permeable particle models¹⁷. Regarding the latter model, the conversion of λ_x to the related reduced hydrodynamic radius parameter γ in the spherical annulus model was done using Eq. (8) for $D_0^l(\lambda_x)$. This corresponds to the inversion of the curve for λ_x^l in Fig. (4) in terms of γ . For example, the smallest reasonably selected value $\lambda_x = 0.1$ corresponds to $\gamma = 0.89$. Results for D_S are depicted in Fig. 6 in dependence on the reduced slip length $\bar{\gamma}$, for volume fractions extending over a broad concentration range.

The excellent agreement between the scaling formula for D_S (solid lines) and the simulation data (symbols) does not only validate this formula. For the special case of permeable hard spheres, it additionally highlights the good performance of the HRM, for a broad concentration range and permeability values largely exceeding the ones discussed earlier in the thin shell-limit discussion of the core-shell model in Ref.²².

In summary, the analytic formula in Eqs. (26) and (27) allows for a quick and accurate calculation of the translational short-time self-diffusion coefficient of hydrodynamically structured spherical particles with hard-core interactions. The only input is the single-particle property a_h/a which can be determined experimentally, e.g., by a DLS measurement of D_0^l in conjunction with a static scattering experiment determining the excluded volume radius. The formula for D_S is applicable also to particles with a short-range, weakly soft pair potential such as the Hertz potential for non-small potential strengths ε , provided the effective diameter σ_s and the related volume fraction ϕ_s are used instead of σ and ϕ .

The formula for D_S in Eqs. (26) and (27) based on its virial expansion is not valid for particles with a long-range, soft pair potential where an (effective) excluded volume diameter is not the characteristic parameter. An example in case are low-salinity suspensions of charge-stabilized colloidal spheres, where according to theory, simulation and experiment D_S has to good accuracy the fractional concentration dependence $D_S/D_S^0 - 1 \approx A_S \phi^{4/3}$, with a coefficient $A_S \approx 2.5 - 2.9$ which varies to a small extent with the particle size and charge^{67,75}. The initial slope of D_S at $\phi = 0$ is thus zero in these charge-stabilized systems. Different from the formula in Eqs. (26) and (27), the HRM is applicable also to spherical particles with arbitrary soft direct interactions, and to particles of fuzzy hydrodynamic structure without a sharp outer boundary. In the framework of the HRM, the coefficient D_S and other short-time transport properties of particles with soft interactions can be approximately and semi-analytically calculated using the PA method at smaller and the self-part corrected $\delta\gamma$ method at larger concentrations. The inputs $g(r)$ and $S(q)$ to these methods can be obtained from Ornstein-Zernike integral equation schemes such as the analytical scheme for charge-stabilized particles introduced in Refs.^{76,77}.

3.3 Sedimentation coefficient

Different from self-diffusion, the neglect of hydrodynamic near-distance and particularly lubrication effects in approximate analytic calculations is less consequential regarding sedimentation. Therefore, K can be described semi-qualitatively on the Rotne-Prager (RP) type level where only the long-distance dipolar contribution to the mobility tensors is accounted for. This amounts hydrodynamically to the neglect of all hydrodynamic flow reflection by the particles.

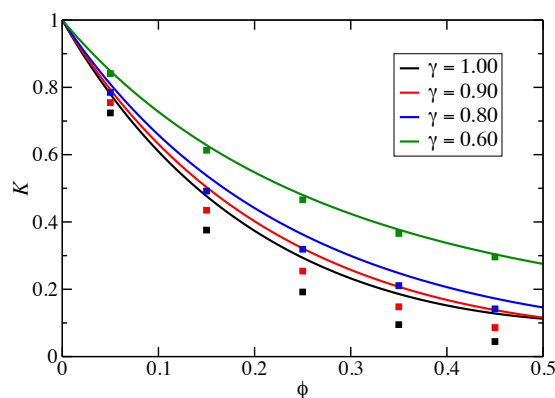


Fig. 7 Concentration dependence of the sedimentation coefficient, K , of the spherical annulus model for reduced hydrodynamic radius values γ as indicated. Solid lines: RP approximation K_{RP} in Eq. (28). Filled symbols: Simulation data taken from Ref.²¹.

Using the RP approximation in conjunction with the analytic PY solution for the Laplace transform of $r g(r)$, Contreras-Aburto *et al.*⁷⁸ have derived analytic expressions for the short-time sedimentation coefficient of Navier partial-slip and uniformly permeable spheres with hard-core interaction. Here, we present the according expression for spherical annulus particles,

$$K_{RP}(\phi, \gamma) = 1 + \gamma\phi \left(\gamma^2 + 12 \left[\frac{\phi(2-\phi) - 10}{20(1+2\phi)} \right] \right), \quad (28)$$

which includes hydrodynamic point particles as a limiting case for which $K(\phi, \gamma = 0) = 1$. In the opposite limit, $\gamma = 1$, of no-slip hard spheres, Eq. (28) reproduces an expression by Banchio and Nägele⁶⁷ which was rederived subsequently by Gilleland *et al.*⁷⁹ using a variational method.

The comparison in Fig. 7 of the RP based analytic formula in Eq. (28) with benchmark simulation data for spherical annulus hard spheres²¹ shows that the sedimentation velocity is overestimated by the formula at larger concentrations. This is a consequence of the neglect of flow reflections in the RP

approximation which becomes less severe with decreasing annulus parameter γ , owing to the for a fixed ϕ increasing distances between the hydrodynamic particle surfaces. For the lowest considered value $\gamma = 0.6$, excellent agreement between the simulation data and K_{RP} is observed. The largest deviations occur for no-slip hard spheres where K_{RP} provides an upper bound to the exact sedimentation coefficient^{62,79}. As an aside, we note that even at $\phi = 0.5$, K_{RP} changes only slightly if the VW-corrected $g(r)$ is used instead of the bare PY $g(r)$.

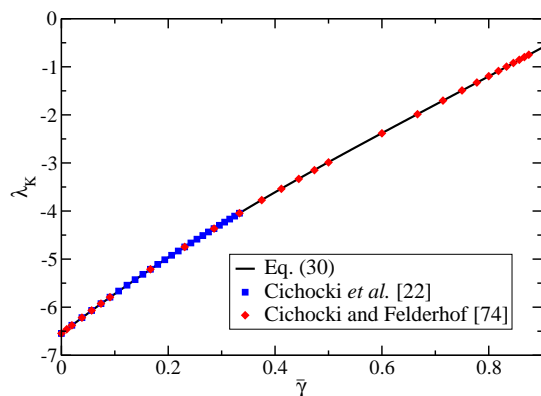


Fig. 8 First-order virial coefficient, λ_K , of the sedimentation coefficient of spherical annulus particles. Filled symbols: Tabulated values by Cichocki *et al.* for thick (diamonds)⁷⁴ and thin annulus shell (squares) systems²², in comparison with the polynomial in Eq. (30) (black solid line).

While K_{RP} nicely describes the trends of the exact spherical annulus sedimentation coefficient K in its ϕ and γ dependence, in search of an improved analytic expression we make the ansatz

$$K(\phi, \gamma) = 1 + \lambda_K(\gamma) u_K(\phi, \gamma) \quad (29)$$

$$= 1 + \lambda_K(\gamma) \phi [1 + \mathcal{O}(\phi)],$$

where $\lambda_K(\gamma)$ is the first-order virial coefficient of the sedimentation coefficient for which high-precision values have been provided by Cichocki *et al.*^{22,74}. According to Fig. 8, these tabulated values are well represented by the polynomial,

$$\lambda_K(\gamma) = -6.5464 + 8.592\bar{\gamma} - 3.901\bar{\gamma}^2 \quad (30)$$

$$+ 2.011\bar{\gamma}^3 - 0.142\bar{\gamma}^4$$

in the full parameter range $0 < \gamma \leq 1$. At $\gamma = 1$ in particular, the known value $\lambda_K = -6.5464$ of no-slip hard spheres is recovered from the polynomial.

In the first equality in Eq. (29), we have introduced the sedimentation scaling function $u_K = (K - 1)/\lambda_K$. In Ref.³⁴, a

scaling ansatz analogous to Eq. (29) was used for the short-time translational and rotational self-diffusion coefficients of uniformly permeable hard spheres. By the comparison with simulation data, it was shown therein that the scaling functions $u_S(\phi, \lambda_x)$ and $u_R(\phi, \lambda_x)$ associated with translational and rotational self-diffusion, respectively, are practically independent of the permeability coefficient for all values $\lambda_x \leq 0.1$. They are therefore well approximated by (i.e. scaled to) the respective functions $u_{S,R}(\phi, \lambda_x = 0)$ of non-permeable solid spheres. On using a third-order polynomial fit of $u_S(\phi, \lambda_x = 0)$ obtained from simulation data of no-slip hard spheres, and the first two known virial coefficients of $D_S(\phi, \lambda_x = 0)$, Eq. (26) for $D_S(\phi, \lambda_x)$ has been obtained^{34,42}.

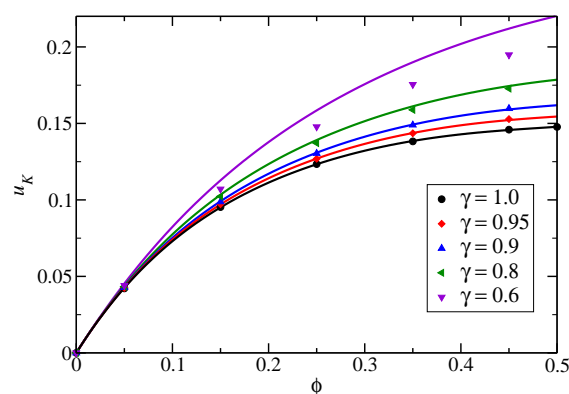


Fig. 9 Concentration dependence of the scaling function $u_K(\phi, \gamma)$ associated with the sedimentation coefficient of spherical annulus particles, for values of γ as indicated. Colored closed symbols: Values obtained from simulation data of $K(\phi, \gamma)$ ²¹. Colored solid lines: Semi-empirical formula in Eq. (31).

As noticed already in the context of permeable spheres³⁴, u_K depends significantly on the intra-particle hydrodynamic structure, different from its self-diffusion siblings. In Fig. 9, this is demonstrated for the spherical annulus system using tabulated simulation data for $K(\phi, \gamma)$ in Ref.²¹. The simulation data of $u_K(\phi, \gamma)$ for a fixed $\phi > 0$ clearly differ from each other for different γ values. Thus, the γ -dependence of $K(\phi, \gamma)$ cannot be embodied solely in terms of the first-order virial coefficient, in contrast to Eq. (26) describing D_S . However, as it is shown in Fig. 9, the simulation data for u_K are well described for $\gamma \geq 0.8$ by a forth-order polynomial in $\gamma\phi$, namely

$$u_K(\phi, \gamma) = \phi \left[1 - 3.348\gamma\phi + 7.426(\gamma\phi)^2 \quad (31)$$

$$- 10.034(\gamma\phi)^3 + 5.882(\gamma\phi)^4 \right].$$

The resulting analytic expression,

$$K(\phi, \gamma) = 1 - \lambda_K(\gamma) \phi \left[1 - 3.348\gamma\phi + 7.426(\gamma\phi)^2 - 10.034(\gamma\phi)^3 + 5.882(\gamma\phi)^4 \right], \quad (32)$$

for the sedimentation coefficient provides in conjunction with Eq. (30) for $\lambda_K(\gamma)$ an accurate description in the from the experimental viewpoint sufficiently broad parameter range $\gamma \in \{0.8 - 1\}$. The numerical coefficient 3.348 in the bracket of Eq. (32) is selected such that at $\gamma = 1$ the correct numerical value 21.918 of the second virial coefficient of no-slip rigid spheres⁷⁴ is recovered.

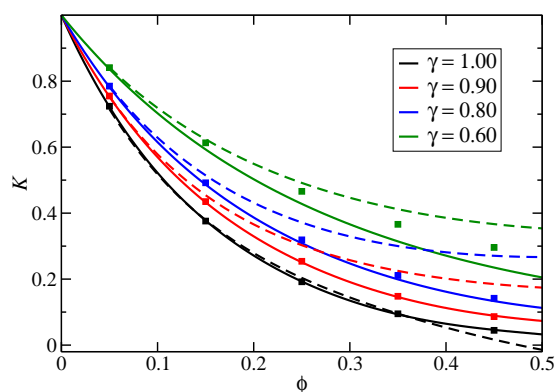


Fig. 10 Sedimentation coefficient of the spherical annulus model as a function of ϕ , for values of γ as indicated. Filled squares: Simulation data for spherical annulus particles²¹. Solid lines: Analytic formula in Eq. (32) with λ_K according to Eq. (30). Dashed lines: Self-part corrected $\delta\gamma$ method prediction, with self-part D_S according to Eq. (26) and VW-PY input for $S(q)$.

From Fig. 10, the good agreement of the semi-empirical formula for $K(\phi, \gamma)$ in Eq. (32) with the spherical annulus simulation data²¹ is noticed for $\gamma \geq 0.8$. The figure depicts also simulation data for permeable spheres where λ_K has been converted to the respective γ using Eq. (8). Moreover, results for $K(\phi, \gamma)$ are displayed as predicted by the self-part corrected $\delta\gamma$ scheme with VW-PY structure factor input where the self-part contribution to K was calculated according to Eq. (26). See Appendix B for details on the $\delta\gamma$ method of calculating $H(q)$ and its self-part correction. While in good overall agreement with the simulation data, the self-part corrected $\delta\gamma$ method results for K deviate significantly at larger ϕ . Different from Eq. (32) which applies to spherical particles with hard-core interactions only, the $\delta\gamma$ method is applicable also to particles with soft interactions.

The analytic expressions in Eqs. (32) and (26) for K and D_S are profitably used in the following discussion of the hydrodynamic function of core-shell particle systems.

3.4 Hydrodynamic function scaling

Due to the fact that $H(q)$ is given according to Eq. (20) by an equilibrium average over hydrodynamic mobilities, its principal peak location and the wavenumber locations of its secondary maxima are nearly coincident with those of $S(q)$. As a static equilibrium property, $S(q)$ is independent of the hydrodynamic particle structure and the HIs in general. This observation has led Abade *et al.* to the following remarkable finding¹⁸, which they analyzed in the context of uniformly permeable hard spheres: While the amplitudes of the oscillations in $H(q)$ are strongly sensitive to the permeability (i.e., the hydrodynamic particle structure), the relative q -dependence of $H(q)$ is practically permeability independent and can be scaled thus to that of no-slip hard spheres. To see this quantitatively, consider the so-called reduced hydrodynamic function¹⁸,

$$h_d(q) = \frac{H_d(q)}{|H_d(q=0)|}, \quad (33)$$

where $H_d(q)$ is the wavenumber-dependent distinct part of $H(q)$ introduced in Eq. (21).

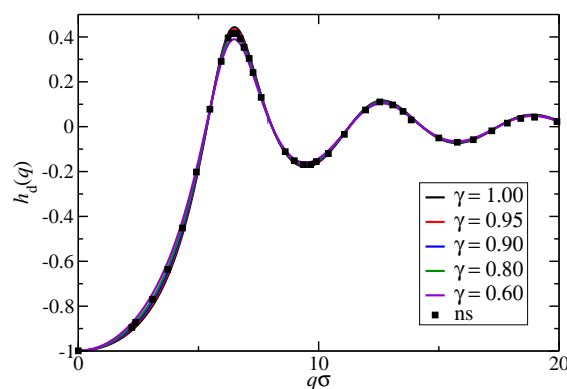


Fig. 11 Reduced hydrodynamic function, $h_d(q)$, for spherical annulus particles at fixed volume fraction $\phi = 0.35$ and varying γ as indicated. The wavenumber is scaled in terms of the hard-sphere diameter $\sigma = 2a$. Solid lines: $\delta\gamma$ method results using VW-PY structure factors as input (cf. Appendix B). Filled squares: Simulation result for no-slip (ns) hard spheres ($\gamma = 1$) taken from Ref.¹⁸.

The reduced hydrodynamic function is defined such that $h_d(q=0) = -1$ and $h_d(q \rightarrow \infty) = 0$. Abade *et al.* found that

$h_d(q)$ is at all q nearly independent of the permeability parameter λ_v , practically in the complete liquid-phase concentration interval. In extrapolating their finding to the spherical annulus model as motivated by our general discussion in Subsec. 2.2, $H(q)$ can be expected to be well represented by

$$H(q) \approx \frac{D_S(\phi, \gamma)}{D_0^t(\gamma)} + h_d^{ns}(q) \left[K(\phi, \gamma) - \frac{D_S(\phi, \gamma)}{D_0^t(\gamma)} \right], \quad (34)$$

where $h_d^{ns}(q) = h_d(q, \gamma = 1)$ is the reduced hydrodynamic function of no-slip hard spheres. The hydrodynamic particle structure enters into this expression by the coefficients K and D_S/D_0^t only for which we have provided accurate analytic expressions. The relative q -dependence of $H(q)$ is described by the master function $h_d^{ns}(q)$ which can be conveniently calculated using the semi-analytic $\delta\gamma$ method for $H_d(q)$. The $\delta\gamma$ method has been shown, in comparison to Stokesian dynamics simulations, to give quite accurate predictions not only for the $H_d(q)$ of no-slip hard spheres⁴², but likewise for charge-stabilized suspensions with long-range electrostatic interactions^{42,68}. To validate hydrodynamic function scaling for the

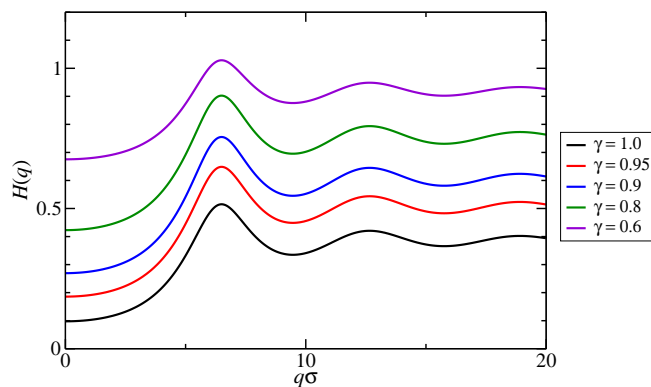


Fig. 12 Hydrodynamic function, $H(q)$, of spherical annulus spheres for $\phi = 0.35$ and values of γ as indicated. The solid lines show results by the semi-analytic formula in Eq. (34), with D_S/D_0^t and K according to Eqs. (26) and (32), respectively, and $h_d^{ns}(q)$ calculated using the $\delta\gamma$ method.

spherical annulus model, in Fig. 11 we present results for $h_d(q, \gamma)$ in a broad γ parameter range, obtained using the $\delta\gamma$ method in Appendix B. All curves collapse practically on a single master curve which in turn nicely agrees with the simulation data for no-slip (ns) hard spheres taken from Ref.¹⁸.

The sensitivity of $H(q)$ on the reduced hydrodynamic radius γ is illustrated in Figure 12, where $H(q)$ has been calculated according to Eq. (34). The strength of the HIs ceases with decreasing γ . Notice that $H(q) \rightarrow 1$ for $\gamma \rightarrow 0$.

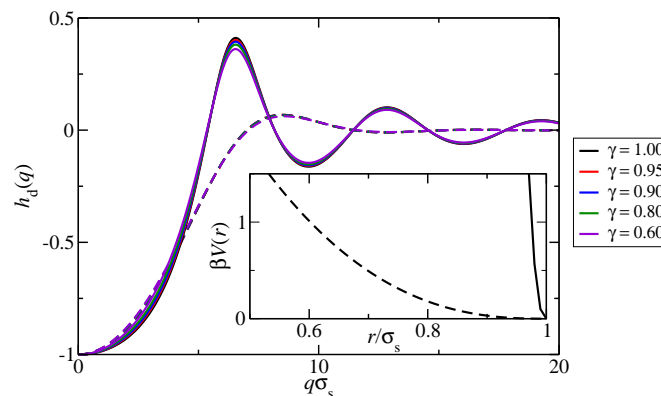


Fig. 13 Reduced hydrodynamic function, $h_d(q)$, for a Hertzian spheres system of interaction strength $\varepsilon = 10$ (dashed lines) and $\varepsilon = 10^4$ (solid lines), respectively, for various reduced hydrodynamic radii, $\gamma = a_h/a_s$, as indicated. The effective volume fraction is $\phi_s = 0.35$. The depicted results have been calculated using the $\delta\gamma$ method with PY structure factor input. Inset: Excerpt of the Hertz potential curve for $\varepsilon = 10$ (dashed) and $\varepsilon = 10^4$ (solid), respectively. Wavenumber q and radial distance r are scaled by the effective soft diameter, $\sigma_s = 2a_s$, of the Hertz potential.

To date, the validity of the hydrodynamic function scaling was scrutinized for particles with hard-sphere interactions only^{17,18}. As discussed in Subsec. 2.1, the soft Hertz potential in Eq. (1) is a useful description of the coarse-grained interaction of certain types of mechanically soft microgel particles. For this reason, we investigate now the scaling of the hydrodynamic function for suspensions of Hertz particles of different interaction strengths ε . In Fig. 13, the functions $h_d(q)$ of Hertz particles are shown for various values of the reduced hydrodynamic radius, defined here by $\gamma = a_h/a_s$ with $a_s = \sigma_s/2$ denoting the effective soft radius of the Hertz potential. Two largely distinct interaction (softness) parameters $\varepsilon = 10$ and 10^4 are considered, representing highly soft and weakly soft particle systems, respectively. The inset depicts the respective shapes of the Hertz potential. For $\varepsilon = 10$, there is a significant likelihood of finding two particles at a distance smaller than σ_s , as quantified by values of $g(r < \sigma_s)$ significantly larger than zero. Even then the HRM remains applicable, provided the hydrodynamic structure of the actual soft particles is not significantly distorted away (on average) from spherical symmetry during particle interpenetration.

The curves for $h_d(q)$ in Fig. 13 have been obtained using the HRM-based $\delta\gamma$ method with the structure factor input for the Hertzian spheres calculated in PY approximation. The figure shows that hydrodynamic function scaling applies to Hertz model particles for a broad softness range, with the shape of

the γ -independent master curve for $h_d(q)$ depending on the softness parameter. The scaling behavior of $H(q)$ can be expected to hold also for other soft pair potentials.

3.5 High-frequency viscosity

So far diffusion related properties have been addressed only. We discuss next a short-time rheological property, namely the high-frequency-limiting suspension viscosity, η_∞ , which linearly relates the average suspension shear stress to the applied rate of strain in a low-amplitude, high-frequency shear experiment. Like the short-time diffusion properties discussed before, η_∞ is a quantity of purely hydrodynamic origin, influenced by direct particle interactions through the equilibrium averaging only. For particles acting hydrodynamically like points ($\gamma = 0$), it reduces thus to the shear viscosity, η_0 , of the suspending Newtonian fluid.

The high-frequency viscosity should be distinguished from the zero-frequency viscosity⁸⁰,

$$\eta(\phi) = \eta_\infty(\phi) + \Delta\eta(\phi), \quad (35)$$

determined in a steady low-shear experiment. The zero-frequency viscosity η has an additional contribution, $\Delta\eta > 0$, originating from the relaxation of the shear-distorted dynamic particle cage formed around each particle. The shear relaxation part $\Delta\eta$ is influenced both by direct and hydrodynamic interactions, with the consequence that for strongly correlated colloidal particles it is substantially larger than η_∞ . An analytic method of calculating the long-time transport property η is presented in Subsec. 5.2.

In Refs.^{18,20}, a generalized Saitô formula for the high-frequency viscosity of permeable spheres with hard-core interactions has been introduced which for $\phi \leq 0.5$ gives results in good agreement with simulation data. In the framework of the spherical annulus model, the formula reads

$$\frac{\eta_\infty(\phi, \gamma)}{\eta_0} = 1 + [\eta](\gamma)\phi \frac{1 + \hat{S}(\phi, \gamma)}{1 - \frac{2}{5}[\eta](\gamma)\phi(1 + \hat{S}(\phi, \gamma))}. \quad (36)$$

It expresses η_∞ in terms of the intrinsic viscosity, $[\eta](\gamma) = (5/2)\gamma^3$, depending on the hydrodynamic particle structure only, and the Saitô function $\hat{S}(\phi, \gamma)$. The latter is approximated linearly in ϕ as

$$\hat{S}(\phi, \gamma) = \left(\frac{\lambda_V(\gamma)}{[\eta](\gamma)} - \frac{2}{5}[\eta](\gamma) \right) \phi, \quad (37)$$

where $\lambda_V(\gamma)$ is the first-order virial coefficient in the expansion of η_∞/η_0 in powers of ϕ . Numerical values for the first virial coefficient of spherical annulus particles are given in Ref.²². For $\gamma \geq 2/3$, these values are well represented by the

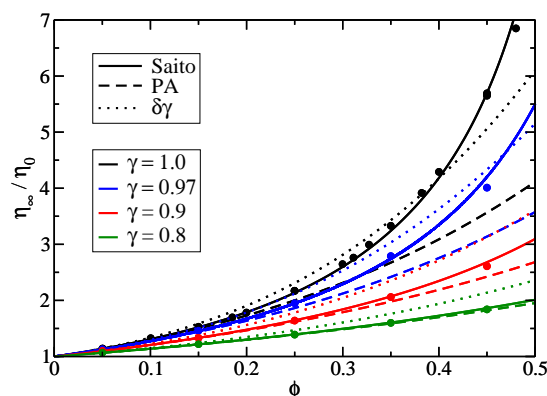


Fig. 14 High-frequency viscosity, η_∞ , of spherical annulus particles in dependence on ϕ , for values of γ as indicated. Filled symbols: Simulation data taken from Refs.^{21,67}. Solid lines: Generalized Saitô formula in Eqs. (36) - (38). Dashed lines: PA scheme results with VW-PY input for $g(r)$. Dotted lines: $\delta\gamma$ scheme results with VW-PY input for $S(q)$.

polynomial

$$\lambda_V(\gamma) = 5.0021 - 39.279\bar{\gamma} + 143.179\bar{\gamma}^2 - 288.202\bar{\gamma}^3 + 254.581\bar{\gamma}^4. \quad (38)$$

In Fig. 14, the predictions for η_∞ by the generalized Saitô formula in Eqs. (36) - (38) are compared with existing simulation results²¹ for the spherical annulus model. There is good agreement with the simulation in the displayed liquid-phase concentration range. For fixed concentration n and fixed hard-core radius a_h , i.e. increasing γ , owing to the enlarged dissipation. Additionally shown in the figure are results for η_∞ by the PA and $\delta\gamma$ methods described in Appendices A and B, respectively. Like in the PA scheme for short-time diffusion properties, two-body HIs contributions to η_∞ are fully accounted for but three-body and higher order contributions have been neglected. The PA scheme is in good agreement with the simulation data for $\phi < 0.2$ only. For small γ , the applicability of the PA method extends to somewhat larger ϕ . We attribute this first to the weaker hydrodynamic interactions for $\gamma < 1$, and second to the fast $\mathcal{O}(1/r^6)$ asymptotic decay of the shear mobility function associated with η_∞ (see Appendix A). While the $\delta\gamma$ scheme viscosity predictions for no-slip spheres are in better agreement with the simulation data than those by the PA scheme, for $\gamma < 1$ the $\delta\gamma$ scheme consistently overestimates the high-frequency viscosity. Quite interestingly, for all $\phi < 0.5$ the $\delta\gamma$ prediction for η_∞ scales to good accuracy with the hydrodynamic volume fraction $\phi_h = \gamma^3\phi$.

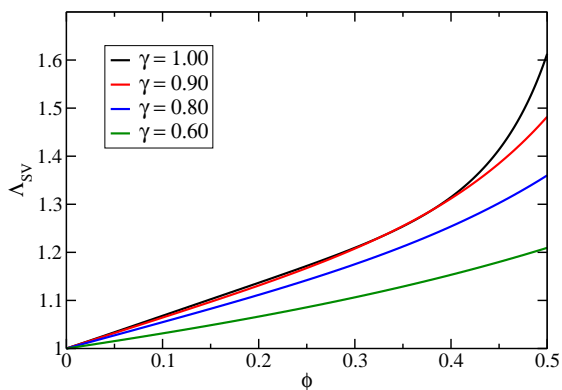


Fig. 15 Test of the short-time GSE relation in Eq. (39) for spherical annulus particles with values of γ as indicated. Solid lines: Product function Λ_{SV} of the generalized Saitô expression in Eq. (36) for η_∞/η_0 and Eq. (26) for D_S/D_0^t in accord with Eq. (40).

As straightforward applications of the generalized Saitô formula and Eq. (26) describing $\eta_\infty(\phi, \gamma)$ and $D_S(\phi, \lambda)$ in the spherical annulus model, we analyze next the validity of the short-time generalized Stokes-Einstein (GSE) relation,

$$\Lambda_{SV}(\phi, \gamma) \approx 1, \quad (39)$$

with the short-time GSE function

$$\Lambda_{SV}(\phi, \gamma) = \frac{D_S(\phi, \gamma)}{D_0^t(\gamma)} \times \frac{\eta_\infty(\phi, \gamma)}{\eta_0}. \quad (40)$$

Eq. (39) expresses that $D_S(\phi, \gamma)$ should be proportional for all concentrations to the inverse of $\eta_\infty(\phi, \gamma)$. This relation is trivially fulfilled at infinite dilution where it reduces to the single-sphere translational Stokes-Einstein relation for a hydrodynamically structured colloidal sphere. The approximate validity of this relation would be quite useful, since η_∞ can then be determined more easily, and using a smaller amount of particles, by a dynamic scattering experiment instead of a rheo-mechanical measurement. This is why GSE relations including the present one have been thoroughly subjected to theoretical explorations, for particulate systems including permeable hard spheres²⁰ and charge-stabilized particles^{38,67}.

An exact GSE relation is reflected in Fig. (15) by a horizontal straight line of unit height. However, for all considered values of γ , significant deviations from $\Lambda_{SV} = 1$ are observed at larger volume fractions. The deviations are largest for no-slip hard-core particles where the HIs are strongest, amounting to about 40% at $\phi = 0.45$. For concentrations $\phi \leq 0.4$, the displayed curves for $\Lambda_{SV}(\phi)$ are nearly straight lines, characterized by the linear coefficient, $\lambda_{SV}(\gamma)$, in the expansion of

Λ_{SV} to linear order in ϕ . The linear concentration coefficient derived from our analytic expressions for D_S and η_∞ is given by the polynomial

$$\lambda_{SV}(\gamma) = 0.6685 + 0.3201\bar{\gamma} + \mathcal{O}(\bar{\gamma}^2). \quad (41)$$

For a given hydrodynamic particle model, the values of γ which should be used in calculating D_S and η_∞ , respectively, are actually different if the $\mathcal{O}(L_{h,f}^*)^2$ corrections to $a_{h,f}$ in Eq. (14) cannot be neglected. However, this does not affect our general conclusion that the GSE relation is violated, as illustrated by the curves in Fig. (15) where for simplicity the same γ values were used in calculating D_S and η_∞ .

According to Fig. (15), the ordering relation $\Lambda_{SV}(\phi) > 1$ is obeyed by particles with pure hard-core interactions. As shown in Ref.⁶⁷, the same ordering applies to charge-stabilized suspensions. In contrast, the long-time product function $\Lambda_{LV}(\phi) = (D_L/D_0^t) \times (\eta/\eta_0)$ relating long-time self-diffusion coefficient D_L to zero-frequency viscosity η has been shown for no-slip hard-sphere and charge-stabilized suspensions to fulfill the opposite ordering $\Lambda_{LV}(\phi) < 1$ for $\phi > 0^{38}$.

4 Theory versus Experiment

We demonstrate now the accuracy of our easy-to-apply toolbox methods of calculating short-time diffusion properties by analyzing DLS measurements by Eckert and Richtering⁴³ on non-ionic PNIPAM microgels in DMF. As discussed in Subsec. 2.1, the microgel particles behave as hard spheres as far as their static properties are concerned. On modeling the microgels also hydrodynamically as no-slip hard spheres with $a_h = a$, and on basis of bare $\delta\gamma$ method results for $H(q)$, Eckert and Richtering came to the conclusion that short-time particle diffusion is underestimated by the no-slip hard-sphere model. This suggests that the non-uniform crosslinker-density of the microgels should have a significant hydrodynamic effect.

To account for this effect, we model here the microgels as spherical annulus particles, and determine $H(q)$ using the scaling Eq. (34) in conjunction with the analytic expressions in Eqs. (32) and (26) for K and D_S , respectively. In the $\delta\gamma$ method calculation of $h_d^{ns}(q)$ which enters into the scaling expression of $H(q)$, we use the HS-PY structure factors depicted in Fig. 1, with the hard-core radius $a = 120$ nm. The only adjustable parameter in our model is thus the reduced hydrodynamic radius $\gamma = a_h/a$.

In Fig. 16, our theoretical results for $H(q)$ are presented and compared with the experimental findings in Ref.⁴³. The latter have been obtained indirectly from dividing the DLS first cumulant data for the diffusion function $D(q)$ by the VW-PY $S(q)$ taken at $q = 0$ (c.f. Eq. (19)). Using the

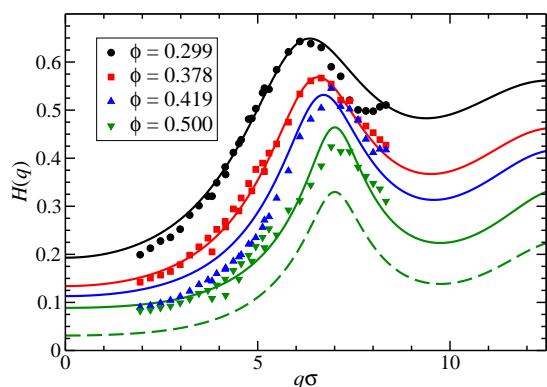


Fig. 16 Experimentally deduced hydrodynamic function of PNIPAM microgels in DMF (filled symbols, taken from Ref. ⁴³) compared with the theoretical predictions (solid lines) for the spherical annulus model, using $\gamma = 0.97$ and Eq. (34) for $H(q)$ combined with Eq. (32) for K and Eq. (26) for D_S . Dashed line: Theoretical prediction for non-permeable particles ($\gamma = 1$) at $\phi = 0.5$. The wavenumbers are scaled by the hard-core diameter $\sigma = 240$ nm.

constant ratio $\gamma = 0.97$, we obtain very good agreement between theory and experiment for all volume fractions. Our finding of a concentration-independent hydrodynamic radius $a_h = 0.97 \times a$ points to the consistency of our analytic method of calculating $H(q)$, since as an intrinsic particle property, a_h should not depend significantly on the volume fraction. While this holds for the strongly cross-linked non-ionic microgels considered here, for weakly cross-linked ionic microgels in the swollen-state temperature range a significant size shrinkage with increasing concentration is observed¹.

The deduced hydrodynamic microgel radius is only 3% smaller than the excluded volume radius, corresponding to a likewise small value, $\lambda_x = 0.029$, of the reduced fluid penetration length. This exemplifies the common experimental situation of $a_h \approx a_{h,f}$, with a relative correction to the flat plane value $a_{h,f}$ being here of $\mathcal{O}((L_{h,f}^*)^2) \approx 10^{-3}$ small.

The small microgel permeability nonetheless significantly affects $H(q)$, in particular at larger concentrations. This is shown in Fig. 16 for $\phi = 0.5$ by the comparison with the hydrodynamic function for zero permeability (dashed curve): The residual particle permeability enlarges the sedimentation velocity by more than 100%, and the self-diffusion coefficient by more than 30%.

In Fig. 17, our theoretical results for $D(q)/D_0^t$ are plotted together with the DLS data⁴³ for the same quantity. The theoretical curves have been obtained from dividing the spherical

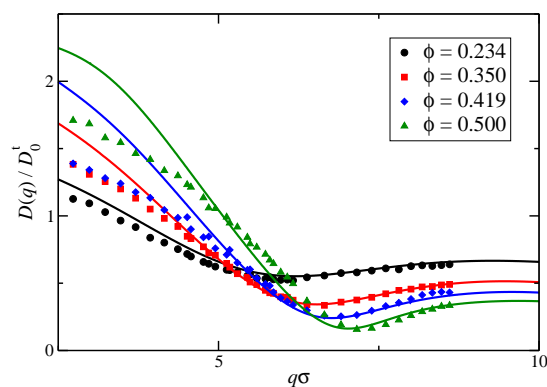


Fig. 17 DLS data for the reduced diffusion function $D(q)/D_0^t$ (filled symbols) taken from Ref. ⁴³, in comparison with our theoretical predictions for $\gamma = 0.97$, obtained by multiplying the spherical annulus results for $H(q)$ depicted in Fig. 16 by the VW-PY values of $S(q = 0)$.

annulus $H(q)$'s depicted in Fig. 16 by the associated VW-PY structure factors, $S(q)$, of hard spheres in accordance with Eq. (19). At $q = 0$, the VW-PY $S(q)$ reduces to the Carnahan-Starling expression for the reduced osmotic compressibility,

$$S(q = 0) = \frac{(1 - \phi)^4}{(1 + 2\phi)^2 + \phi^3(\phi - 4)}, \quad (42)$$

valid in the full fluid-phase volume fraction range of hard spheres. The agreement between theoretical and experimental diffusion functions is very good in the intermediate wavenumber range including the principal peak position, q_m , of $S(q)$ where $D(q)$ is minimal, and also for larger wavenumbers. At small q values and large volume fractions, the experimental data are overestimated. Even considering the remaining small- q deviations, the here presented theoretical results for $D(q)$ are in distinctly better agreement with the experimental data than the earlier ones presented in Ref. ⁴³ where permeability effects were not included.

The deviations in $D(q)$ at small- q can be partially attributed to the high sensitivity of the inverse compressibility factor, $1/S(0)$, multiplying $H(0)$ in Eq. (23), on the residual softness of the microgels. This is demonstrated in Fig. 18, where the concentration dependence of $1/S(0)$ for hard spheres is compared to that of the Hertz potential system for the strongly distinct softness parameters $\varepsilon = 10^4$, 10^2 and 10. According to the figure, even a small residual softness characterized by $\varepsilon = 10^4$ significantly enlarges the osmotic compressibility for large volume fractions, with $1/S(0)$ being lowered accordingly. Viewed on the scale of the structure factors in Fig. 2, the

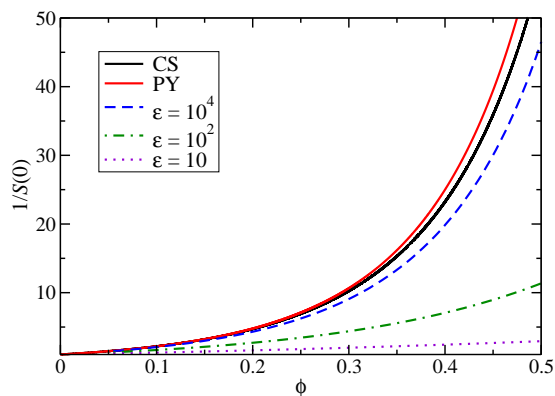


Fig. 18 Influence of particle softness (elasticity) on the inverse compressibility factor $1/S(0)$, for hard-sphere and Hertz potential particles, plotted as a function of ϕ . The Carnahan-Starling (CS) (black solid line) and PY (red solid line) results for hard spheres are compared with the PY-based predictions for Hertz model particles with softness parameters $\varepsilon = 10^4$ (dashed line), 10^2 (dashed-dotted line), and 10 (dotted line).

small- q differences are not resolved since $S(0)$ is very small for large concentrations. While the smaller factor $1/S(0)$ in the Hertz model would improve the agreement with the experimental $D(q)$ at small q , we recall in referring to Fig. 2 that a somewhat larger volume fraction ϕ , than for hard spheres is required in the Hertz model for an equally good fit of the experimental $S(q)$. If the enlarged volume fraction is accounted for, there remains a small final reduction in $1/S(0)$ only. An additional cause for the small- q differences can be size polydispersity. It was shown in Ref.⁸¹, that a small degree of polydispersity significantly enlarges in concentrated suspensions the measured diffusion function at small q .

In summarizing, we conclude that our HRM based toolbox methods reproduce the short-time diffusion properties of the non-ionic microgel suspensions very well, and with little numerical effort. The non-homogeneous cross-linker density is accounted for by a hydrodynamic radius which is only three percent smaller than the excluded volume radius.

5 Long-time Transport Properties

Long-time colloidal transport properties such as D_L and η characterize the particle dynamics on time scales $t \gg \tau_D$ during which the particle configuration has changed significantly. Different from short-time properties, they are influenced by thermally driven microstructural relaxations depending on direct and hydrodynamic interactions alike. This renders a first-principles calculation of long-time properties demanding, both

in theory and simulations, in particular when the salient HIs are accounted for. Consequently, in most simulation studies of the concentration dependence of D_L and η , the influence of the HIs has been ignored^{82–84}. The few existing three-dimensional simulation studies where HIs are included have been focused on Brownian hard spheres with no-slip BC^{85–87}. Therefore, a theoretical scheme is in demand allowing for the approximate calculation of D_L and η for suspensions of hydrodynamically structured particles.

In the following, we present such a scheme which as a bonus requires only little numerical effort. It is based on the HRM and a factorization approximation method proposed originally by Medina-Noyola for self-diffusion³⁵. We point out that the HRM error estimation for short-time properties in Eq. (25) applies also to long-time properties including D_L/D_0^t and η , and also the dynamic structure factor $S(q,t)$ for arbitrary correlation times. This follows from general expressions for long-time transport coefficients and $S(q,t)$ which have been obtained using the Mori-Zwanzig projection operator formalism in conjunction with the many-particle generalized Smoluchowski equation for the configurational probability distribution function³¹. The crucial fact to notice here is that the hydrodynamic mobility tensors entering into the GSmE have no explicit time dependence.

We exemplify the error estimate for D_L by starting from the configurational average expression³¹,

$$D_L = D_S + \Delta D, \quad (43)$$

with

$$\Delta D = -\langle (\hat{\mathbf{q}} \cdot \mathbf{V}_1) \mathcal{O}_B^{-1} (\hat{\mathbf{q}} \cdot \mathbf{V}_1) \rangle. \quad (44)$$

The slowing effect on D_L by the dynamically restructuring cage of next neighbors formed around each particle is embodied in the negative valued relaxation contribution, ΔD , to D_L implying $D_L < D_S$ for $\phi > 0$. In Eq. (44), $\mathbf{V}_1 = \mathcal{O}_B \mathbf{R}_1$ is the coarse-grained velocity of a representative particle 1 whose Brownian motion is considered, $\hat{\mathbf{q}} = \mathbf{q}/q$, and $\mathcal{O}_B(\mathbf{X})$ the so-called backward Smoluchowski differential operator generating the time evolution of the probability distribution function. The operator inverse is denoted by \mathcal{O}_B^{-1} . The only information about \mathcal{O}_B needed here is its linear dependence on the mobility tensors $\boldsymbol{\mu}_{ij}$. From this and Eq. (24), it follows that the error introduced on approximating D_L/D_0^t by $D_{L,\text{HRM}}/D_0^t$ is of $\mathcal{O}((L_{h,f}^*)^2)$.

5.1 Long-time self-diffusion

Using Eq. (43), D_L can be written as

$$D_L(\phi) = D_S(\phi) \left[1 + \frac{\Delta D(\phi)}{D_S(\phi)} \right], \quad (45)$$

where in the term in brackets, the explicit dependence on D_S has been scaled out. According to arguments first put forward by Medina-Noyola³⁵, and subsequently substantially elaborated by Brady also regarding the zero-frequency viscosity^{36,37}, the factor function in brackets is not only scale invariant with respect to D_S , but for hard spheres it is to decent approximation also independent of the HIs. This implies the no-HI factorization approximation,

$$\left[1 + \frac{\Delta D}{D_S}\right] \approx \left[\frac{D_L}{D_0^t}\right]_{\text{no-HI}}, \quad (46)$$

where the bracket term is approximated by a purely structural factor determined by excluded volume interactions only. For known D_S , the problem of calculating D_L is thus simplified to the calculation of the reduced long-time self-diffusion coefficient without HIs. The dependence of D_L on the HIs, and the hydrodynamic particle structure, is embodied here in D_S alone.

Brownian dynamics simulation results for $[D_L(\phi)/D_0^t]_{\text{no-HI}}$ by Hinsen and Cichocki⁸² and Moriguchi⁸⁸ are depicted in Fig. 19. In the fluid-phase concentration regime $\phi \leq \phi_f$, where $\phi_f = 0.494$ is the volume fraction at freezing, the simulation data are well described by the polynomial least-square fit,

$$\left[\frac{D_L}{D_0^t}\right]_{\text{no-HI}} = 1 - 2\phi + 1.272\phi^2 - 1.951\phi^3 \quad (47)$$

where the exact first-order virial coefficient, $\lambda_L = 2$, for a hard-sphere suspension without HIs has been incorporated. The figure depicts furthermore the analytic approximation,

$$\left[\frac{D_L}{D_0^t}\right]_{\text{no-HI}} \approx \frac{1}{1 + 2\phi g(\sigma^+; \phi)}, \quad (48)$$

given by Brady³⁶, where the structural factor is expressed in terms of the RDF contact value, $g(\sigma^+; \phi)$, of hard spheres. The contact value for the fluid-phase concentration range is to high accuracy described by the Carnahan-Starling expression⁸⁹

$$g(\sigma^+; \phi) = \frac{1 - \phi/2}{(1 - \phi)^3} \quad (49)$$

with $g(\sigma^+; \phi_f) = 5.81$. Eq. (48) incorporates the exact first-order virial coefficient, $\lambda_L = -2$. Moreover, near random closed packing at $\phi_{\text{rcp}} \approx 0.64$ where a metastable hard-sphere fluid gets jammed, on basis of results for $g(\sigma^+; \phi)$ by Rintoul and Torquato⁸⁹ it predicts that $[D_L]_{\text{no-HI}}$ diminishes linearly like $0.59 \times (1 - \phi/\phi_{\text{rcp}})$. Since D_S vanishes likewise linearly in case of no-slip hard spheres, the quadratic scaling prediction $D_L \sim (1 - \phi/\phi_{\text{rcp}})^2$ near random closed packing is obtained in the factorization approximation.

The performance of the no-HI factorization approximation for the D_L of no-slip spheres on basis of Eq. (26) for D_S at

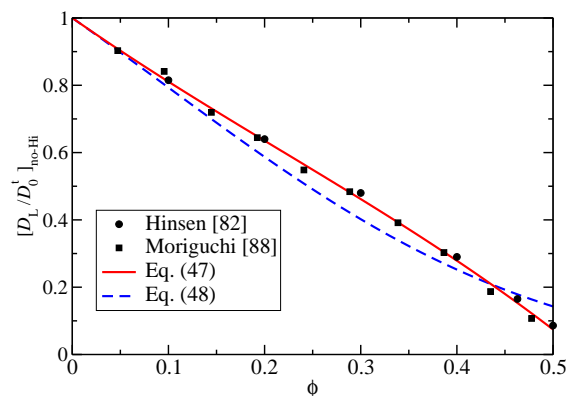


Fig. 19 Reduced long-time self-diffusion coefficient, $[D_L/D_0^t]_{\text{no-HI}}$, of colloidal hard spheres without HIs. Filled circles and squares: Brownian dynamics simulation results by Hinsen and Cichocki⁸² and Moriguchi⁸⁸, respectively. Solid line: Polynomial fit in Eq. (47). Dashed line: Eq. (48) with Carnahan-Starling contact value input.

$\gamma = 1$ and Eq. (47) for $[D_L/D_0^t]_{\text{no-HI}}$, is documented in Fig. 20 by the comparison with DLS data by van Megen *et al.*^{90,91}, and simulation results by Phung *et al.*⁸⁵ with HIs included. The Stokesian dynamics simulation data for Brownian hard spheres by Phung *et al.* have been obtained for a small number ($N = 27$) of particles, and for a small albeit non-zero shear Peclet number $Pe = 0.01$. The overall agreement with the experimental and simulation data is quite good. The factorization approximation gives $\lambda_L = -3.831$ for the first-order virial coefficient of hydrodynamically interacting no-slip spheres, while its correct numerical value is given by $\lambda_L = -2.1$. The initial low-concentration decrease of D_L is thus overestimated.

The good performance of the no-HI factorization approximation for no-slip hard spheres gives support to its straightforward extension to hydrodynamically structured particles, by using for D_S/D_0^t now the analytic expression in Eq. (26) for spherical annulus spheres. Our results for D_L/D_0^t based on this extended factorization scheme are shown in Fig. 21. With decreasing γ , the slowing down effect of the HIs on D_L diminishes. In the limit $\gamma \rightarrow 0$ of hard spheres acting hydrodynamically as point particles, the long-time self-diffusion coefficient in the absence of HIs is recovered. According to Cichocki and Felderhof⁷⁴, the linear concentration coefficient of D_L/D_0^t for small γ is $\lambda_L(\gamma) = -2 [1 - 1.031\gamma + 0.111\gamma^2 + \mathcal{O}(\gamma^3)]$, where the linear and quadratic terms in γ are due to the so-called Oseen long-distance HIs contribution to the relaxation part ΔD . The contributions of the short-time part, D_S , to D_L appear first in quadratic order in γ . While this describes quantitatively how D_L approaches $[D_L]_{\text{no-HI}}$ for small γ , we reem-

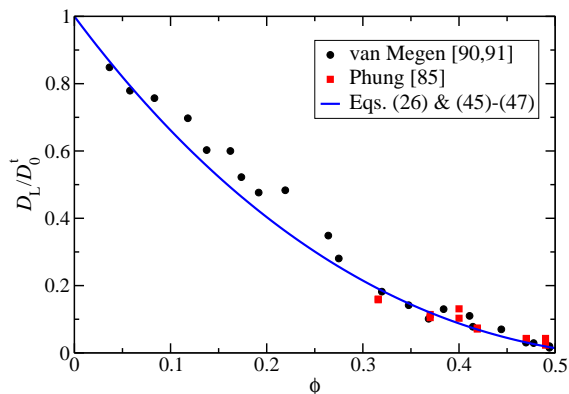


Fig. 20 Reduced long-time self-diffusion coefficient, D_L/D_0^t , of no-slip colloidal hard spheres. Filled circles: Experimental data by van Megen *et al.*^{90,91}. Filled squares: Simulation data by Phung *et al.*⁸⁵. Solid line: No-HI factorization approximation in Eqs. (45)-(47), with the short-time factor D_S/D_0^t according to Eq. (26) for $\gamma = 1$.

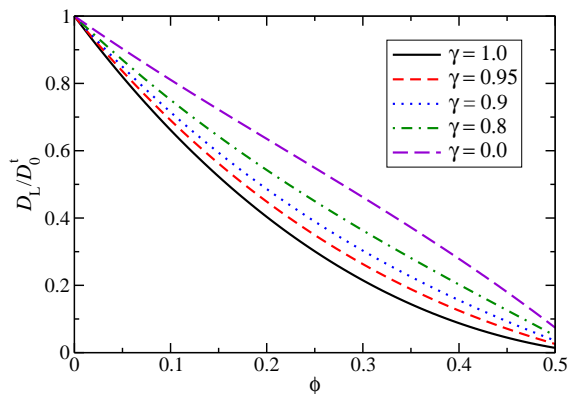


Fig. 21 Generic influence of the intra-particle hydrodynamic structure on D_L/D_0^t , quantified in the no-HI factorization approximation, Eqs. (45)-(47), using for D_S/D_0^t the spherical annulus model formula in Eqs. (26) and (27). Several values of γ are considered as indicated.

phasize that $\gamma > 0.8$ for most hydrodynamically structured colloidal particles.

The no-HI factorization approximation predicts the ratio, D_L/D_S , of long-time and short-time coefficients to be independent of HIs and hydrodynamic particle structure, with value equal to $[D_L/D_0^t]_{\text{no-HI}}$. This implies with Eqs. (45) and (46) that

$$\left(\frac{D_L}{D_S}\right)(\phi_f) \approx 0.1, \quad (50)$$

in good accord with the Löwen-Palberg freezing criterion value of about 0.1. Thus, a universal freezing value of 0.1 is predicted not only for colloidal suspensions with different pair potentials, but also with different hydrodynamic intra-particle structures. For pair interactions characterized by a single length scale, the dynamic Löwen-Palberg criterion has been shown to be equivalent to the static Hansen-Verlet freezing criterion for the value $S(q_m)$ of the structure factor peak height⁶⁵.

5.2 Zero-frequency viscosity

Analogous to Eq. (45) for D_L , in Eq. (35) for the low-shear zero-frequency viscosity η , we factor out the high-frequency (short-time) contribution η_∞ according to

$$\eta(\phi) = \eta_\infty(\phi) \left[1 + \frac{\Delta\eta(\phi)}{\eta_\infty(\phi)} \right], \quad (51)$$

with the term in brackets expected to be approximately independent of the HIs. This suggests the no-HI factorization approximation,

$$\frac{\Delta\eta(\phi)}{\eta_\infty(\phi)} \approx \left[\frac{\Delta\eta(\phi)}{\eta_0} \right]_{\text{no-HI}}, \quad (52)$$

where $[\Delta\eta]_{\text{no-HI}}$ is the shear relaxation viscosity part without HIs. In this approximation, the HIs are assumed to affect η only by means of the factored out η_∞ in Eq. (51). The neglect of HIs simplifies the calculation of the shear relaxation viscosity part considerably. Following works by Brady^{36,37}, an analytic estimate of $\Delta\eta$ for no-slip hard spheres without HIs is given by

$$\left[\frac{\Delta\eta}{\eta_0} \right]_{\text{no-HI}} \approx \frac{12}{5} \phi^2 g(\sigma^+; \phi), \quad (53)$$

with $g(\sigma^+, \phi)$ given by Eq. (49) for $\phi \leq 0.49$. This estimate combines the exact low concentration limit, $2.4\phi^2 + \mathcal{O}(\phi^3)$, of $[\Delta\eta]_{\text{no-HI}}$ with its divergence at random closed packing according to $[\Delta\eta]_{\text{no-HI}} \sim (1 - \phi/\phi_{\text{rcp}})^{-1}$, triggered by the divergence of the hard-sphere contact value. Together with the likewise linear divergence of η_∞ for no-slip hard spheres, a quadratic divergence $\eta \sim (1 - \phi/\phi_{\text{rcp}})^{-2}$ is thus predicted for the zero-frequency viscosity. For hydrodynamically structured particles where $a_h < a$, there are no diverging lubrication

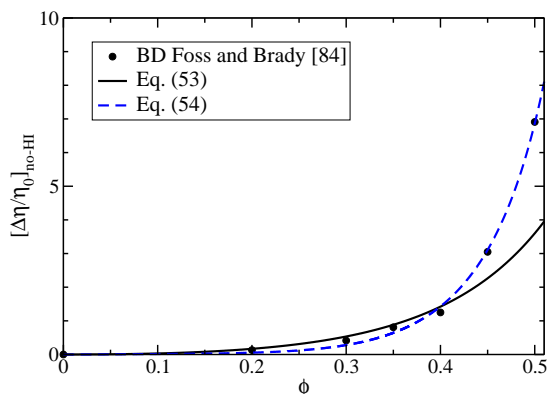


Fig. 22 Reduced shear relaxation viscosity part without HIs, $[\Delta\eta/\eta_0]_{\text{no-HI}}$, of a suspension of Brownian hard spheres in dependence of ϕ . Filled circles: Brownian dynamics (BD) simulation data by Foss and Brady⁸⁴. Solid line: Analytic estimate in Eq. (53). Dashed line: Semi-empirical fit in Eq. (54).

forces for spheres in contact. The high-frequency viscosity remains then finite at random closed packing, and the particles can still rotate individually. Moreover, η diverges only linearly as $\eta(\phi, \gamma < 1) \sim (1 - \phi/\phi_{\text{rcp}})^{-1}$.

In Fig. 22, the outcome of Eq. (53) for $[\Delta\eta]_{\text{no-HI}}$ is compared to Brownian dynamics simulation results without HIs by Foss and Brady^{84,86}. Up to $\phi \approx 0.35$, the simulation data are decently well represented by the analytic expression, but the steep rise of $[\Delta\eta]_{\text{no-HI}}$ at large volume fractions is not reproduced. The simulation data are well captured for all ϕ by the semi-empirical expression

$$\left[\frac{\Delta\eta}{\eta_0} \right]_{\text{no-HI}} = \frac{\frac{12}{5}\phi^2(1 - 7.085\phi + 20.182\phi^2)}{\left(1 - \frac{\phi}{\phi_{\text{rcp}}}\right)}, \quad (54)$$

combining the exact quadratic-order concentration dependence with the linear order divergence at random closed packing. Throughout this work, we restrict our analysis to the equilibrium fluid-phase concentration regime $\phi \leq 0.5$, while the viscosity simulations in Refs.^{83,84,86} have been extended to the metastable fluid concentration regime $\phi_f < \phi < \phi_{\text{rcp}}$ where crystallization is kinetically suppressed. Regarding the shear relaxation viscosity part with HIs included, Brady has proposed the following approximate scaling expression^{36,37},

$$\frac{\Delta\eta}{\eta_\infty} \approx \frac{12}{5}\phi^2 \frac{g(\sigma^+; \phi)}{\Lambda_{\text{SV}}(\phi)}, \quad (55)$$

where the influence of the HIs on the ratio $\Delta\eta/\eta_\infty$ is solely embodied in the short-time GSE function Λ_{SV} defined in Eq.

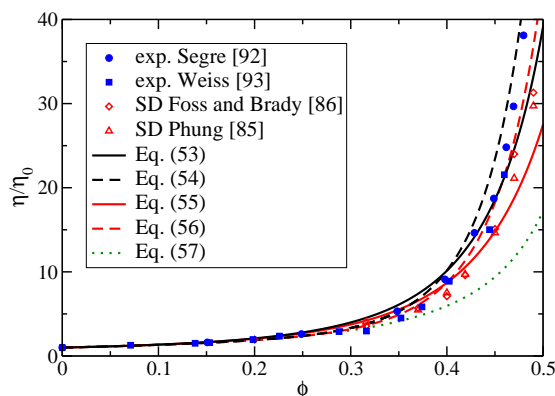


Fig. 23 Zero-frequency viscosity, η/η_0 , of no-slip Brownian hard spheres with HIs. Solid and dashed black lines: No-HI factorization predictions using $\eta_\infty(\phi, \gamma = 1)$ according to Eq. (36), and $[\eta/\eta_0]_{\text{no-HI}}$ according to Eqs. (53) and (54), respectively. Solid and dashed red lines: Brady's (modified) scaling approximations using Eqs. (55) and (56) for $\Delta\eta/\eta_\infty$, respectively, and Eq. (36) for the factored out η_∞ . The factor $1/\Lambda_{\text{SV}}$ in the (modified) scaling approximation is calculated using Eq. (36) for η_∞ and Eq. (26) for D_S . Dotted line: Eq. (57). Filled symbols: Experimental data by Segrè *et al.* and Weiss *et al.*^{92,93}. Open symbols: Stokesian dynamics (SD) simulation results for Brownian hard spheres by Foss and Brady⁸⁶ and Phung⁸⁵.

(40). For no-slip hard spheres, Λ_{SV} is well represented for $\phi < 0.4$ by $\Lambda_{SV} \approx 1 + 0.67\phi$ according to Eq. (41), while without HIs Λ_{SV} is equal to one. Consequently, Eq. (55) predicts $\Delta\eta/\eta_\infty$ to be only mildly affected by the HIs, giving some credit to the no-HI factorization approximation in Eq. (52). Eq. (55) was obtained from arguing that the adequate diffusion time scale in a concentrated suspension is a_h^2/D_s instead of a_h^2/D_0^t , and from using a low-concentration estimate of the weakly shear-distorted stationary pair distribution function with the prefactor $g(\sigma^+; \phi)$ preserved³⁶. A detailed discussion of the approximations going into Eq. (52) is given by Lionberger and Russel^{94,95}.

On using in place of Eq. (53) the semi-empirical fitting expression in Eq. (54) as the non-hydrodynamic factor in Eq. (55), Brady's scaling relation is modified to

$$\frac{\Delta\eta}{\eta_\infty} \approx \frac{\frac{12}{5}\phi^2(1 - 7.085\phi + 20.182\phi^2)}{\left(1 - \frac{\phi}{\phi_{rcp}}\right)\Lambda_{SV}(\phi)}. \quad (56)$$

The two here considered variants of the no-HI scaling approximation of η consist of using Eqs. (53) and (54), respectively, as input for the ratio $\Delta\eta/\eta_\infty$ in the bracket term in Eq. (51), in conjunction with the accurate generalized Saitô formula in Eq. (36) used for η_∞ . In addition, Brady's scaling expression for η and its modification consist of approximating $\Delta\eta/\eta_\infty$ in the bracket term in Eq. (51) by Eqs. (55) and (56), respectively, with the generalized Saitô formula used again for the factored out high-frequency viscosity. The hydrodynamic factor $1/\Lambda_{SV}$ in the two scaling expressions is calculated analytically using Eq. (26) for D_S , and the generalized Saitô formula for η_∞ .

The results for $\eta(\phi, \gamma = 1)$ by the four inter-related analytic approximations are depicted in Fig. 23. They are compared with experimental data by Segrè *et al.*⁹² and Weiss *et al.*⁹³, and Stokesian dynamics (SD) simulation data for Brownian hard spheres with HIs included by Foss and Brady⁸⁶ and Phung *et al.*⁸⁵. The latter have been obtained for a small number ($N = 27$) of particles in the basic simulation box. In Ref.⁸⁶, $\Delta\eta$ was deduced using a general Green-Kubo formula for the shear stress correlation function of hydrodynamically interacting particles⁹⁶. The viscosity curves by all four approximations compare overall quite well with the simulation data. Depending on the used approximation for $\Delta\eta/\eta_\infty$, deviations are visible at intermediate and large volume fractions. The neglect of HIs in $\Delta\eta/\eta_\infty$ results in an overestimation of the simulations data at large ϕ , but the large- ϕ experimental viscosity data are well described. On considering the simulation data to be more trustworthy than the experimental data, owing to experimental polydispersity effects and difficulties in determining the precise volume fraction, the modified scaling expression by Brady in Eq. (56) provides the overall best description of the SD data for η , slightly better than Brady's

original scaling expression in Eq. (55). We use the modified scaling expression in the following discussion of hydrodynamically structured particles. Note that the second-order in concentration coefficient of η is predicted by all four factorization approximation variants as $5.01 + 2.4 = 7.41$, while the exact coefficient is equal to 5.931 ⁹⁷. This low- ϕ difference is not resolved on the scale of Fig. 23.

The figure includes additionally the viscosity prediction by the formula

$$\eta(\phi)/\eta_0 = \frac{1 - 0.4\bar{\phi} + 0.222\bar{\phi}^2}{(1 - \bar{\phi})^2}, \quad (57)$$

with $\bar{\phi} = \phi/\phi_{rcp}$, which incorporates the first two known virial coefficients in $\eta/\eta_0 = 1 + 2.5\phi + 5.91\phi^2 + \mathcal{O}(\phi^3)$ and a quadratic divergence of η at ϕ_{rcp} . As seen in Fig. 23, it describes the simulation and experimental data well for $\phi \leq 0.35$, but it strongly underestimates them at larger ϕ .

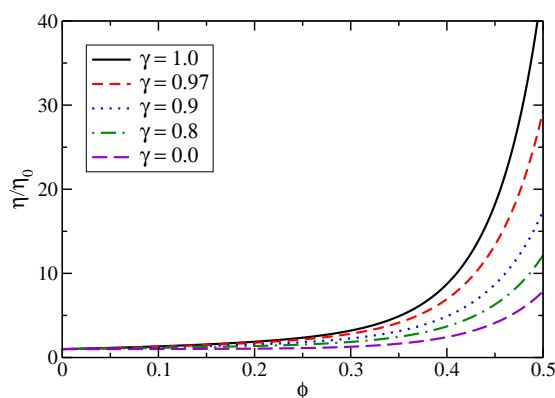


Fig. 24 Predictions for the reduced zero-frequency viscosity, $\eta(\phi, \gamma)/\eta_0$, of hydrodynamically structured particles, based on the modified Brady scaling expression for $\Delta\eta/\eta_\infty$ in Eq. (56), and the generalized Saitô formula in Eq. (36) for $\eta_\infty(\phi, \gamma)$. The hydrodynamic factor $\Lambda_{SV}(\phi, \gamma)$ is calculated using Eq. (36) for $\eta_\infty(\phi, \gamma)$, and Eq. (26) for $D_S(\phi, \gamma)/D_0^t(\gamma)$. Several values of γ are considered as indicated.

Akin to long-time self-diffusion, we can straightforwardly extend our analysis to hydrodynamically structured particles, by using the generalized Saitô expression in Eq. (36) for $\eta_\infty(\phi, \gamma)$, in combination with the modified Brady scaling expression in Eq. (56) for $\Delta\eta/\eta_\infty$. The viscosity predictions for different reduced hydrodynamic radii γ and volume fractions extending up to ϕ_F are depicted in Fig. 24. Note the pronounced reduction of $\eta(\phi, \gamma)$ with decreasing γ , owing to the reduced dissipation, inherited from the similar behavior of $\eta_\infty(\phi, \gamma)$. In the limit $\gamma \rightarrow 0$, the zero-frequency viscosity

reduces to $\eta(\phi, 0) = \eta_0 + [\Delta\eta]_{\text{no-HI}}$. In spite of being approximate, the analytic modified scaling expression for $\eta(\phi, \gamma)$ in Eq. (56) can be expected to be useful for a quick analysis of experimental viscosity data of hydrodynamically structured colloidal suspensions. For the PNiPAM microgels in DMF, e.g., where $\gamma = 0.97$ has been deduced, a significant reduction both in η and η_∞ is predicted relative to the corresponding viscosities of non-permeable particles. It will be interesting to compare our zero-frequency and high-frequency viscosity predictions with future viscosity measurements on non-ionic PNiPAM in DMF systems.

6 Concluding Remarks

We have presented a toolbox of methods for calculating short-time and long-time transport properties of suspensions of spherical particles with intrinsic hydrodynamic structure. The analytic scaling expressions for systems at or near to thermodynamic equilibrium given in the paper combine high accuracy predictions with a practical implementation, and they apply to the full liquid-phase concentration regime. They are useful to experimenters for a fast yet precise data analysis of scattering and rheo-mechanical experiments. We have highlighted this in our analysis of SLS and DLS experiments on non-ionic PNiPAM microgels in DMF. By a detailed comparison with Hertz potential calculations, we have shown that the microgels behave statically to good accuracy as hard spheres, and hydrodynamically as permeable spheres with a reduced penetration length $\lambda_x \approx 0.03$ corresponding to a reduced hydrodynamic radius of $\gamma = 0.97$. It will be interesting to scrutinize the analytic viscosity expressions for η_∞ and η of hydrodynamically structured, rigid spheres against future rheo-mechanical measurements on non-ionic PNiPAM microgels.

The analytic toolbox expressions for the collective diffusion coefficient and the zero-frequency viscosity have been already profitably used in a recent crossflow ultrafiltration study of solvent-permeable nanoparticles suspensions¹¹. The short-time transport coefficient expressions can serve also as input in the calculation of frequency- and time-dependent transport properties on basis of mode-coupling theory and dynamic density functional theory methods where HIs are included^{98,99}. They are likewise useful as input in the context of the empirically observed time-wavenumber factorization scaling of $S(q, t)$ at $q \approx q_m$ for intermediate to long correlation times^{100,101}.

The intra-particle hydrodynamic structure has been accounted for using the hydrodynamic radius model where the particles are described hydrodynamically as no-slip spheres, characterized by a hydrodynamic radius derived from a single-particle transport property for unchanged direct interactions. In spite of its simplicity, the HRM is universally applicable since corrections terms are usually quite small, i.e. of

quadratic order in the reduced slip length. In many particulate systems, these corrections are negligible, and a unique hydrodynamic radius $a_{h,f}$ can be used independent of the considered transport property. As we have shown in comparison with existing computer simulation results, the HRM based scaling expressions for hard-sphere-like particles are decent approximations also for strongly structured particles characterized by values of γ significantly smaller than one, provided a_h is deduced from an associated single-particle transport coefficient, namely from $[\eta]$ in viscosity calculations, and D_0^s in self-diffusion and sedimentation calculations for concentrated suspensions. While our focus has been on monodisperse particle systems, it is feasible to generalize the HRM to size polydisperse particles using an appropriate particle size distribution. In future work, it will be rewarding to search for possible extensions of the scaling relations to polydisperse colloidal systems and mixtures.

Most results presented in this work are for hydrodynamically structured, stiff particles with pure hard-core interactions where the HRM reduces to the spherical annulus model. Part of our toolbox methods are likewise applicable, with appropriate modifications, to spherical particles with short-ranged soft interactions. We have illustrated this in Fig. 13 for the reduced hydrodynamic function, $h_d(q)$, of soft Hertz potential particles with $\varepsilon = 10$. According to our calculations based on the $\delta\gamma$ method, hydrodynamic function scaling remains valid for soft spherical particles. Note here that the self-part corrected $\delta\gamma$ scheme, and the PA approximation for HRM particles, can be used for arbitrary pair potentials.

We finally point to the invalidity of the presented scaling relations for D_S , K , and D_L for particles with long-range soft repulsion that are not adequately described by an effective excluded volume diameter. Examples in case are low salinity suspensions of charge-stabilized particles⁷⁵, and quasi-two dimensional systems of magnetically repelling particles at a liquid-gas interface¹⁰². As shown both in computer simulations and experiments, D_S and K in these systems follow a fractal $\sim \phi^{4/3}$ and $\sim \phi^{1/3}$ concentration dependence, respectively, of zero and negative infinite initial slope^{67,75}. Moreover, the factorization scaling relation in Eqs. (45) and (46) predicting that $D_L < [D_L]_{\text{no-HI}}$ does not apply to these long-range repulsive systems where, on the contrary, a hydrodynamic enhancement of long-time self-diffusion is observed in theory⁹⁸, simulation^{65,103} and experiments¹⁰². The short-time self-diffusion coefficient in these systems is only weakly affected hydrodynamically at lower concentrations so that $D_S \approx D_0^s$. The major effect originates instead from the relaxation part ΔD whose magnitude is lowered by the here dominating far-field part of the HIs⁹⁸. While the scaling expressions are invalid, the hydrodynamic structures of the low-salinity charge-stabilized and magnetic particles is still well described by the HRM. On basis of the HRM the short-time properties

of hydrodynamically structured charge-stabilized particles can be calculated using the self-part corrected $\delta\gamma$ scheme in conjunction with the PA method for the self-part.

Acknowledgements

J.R. acknowledges support by the International Helmholtz Research School on Biophysics and Soft Matter (IHRS BioSoft). G.N. and J.R. thank M. Heinen (CalTech, Pasadena), B. Cichocki (Warsaw University), and M. Ekiel-Jezewska and E. Wajnryb (Polish Academy of Sciences, Warsaw) for many helpful discussions. This work was partially funded by the Deutsche Forschungsgemeinschaft (DFG) within the framework of the SFB-985 (project B6).

A Pairwise-additivity (PA) approximation applied to the HRM

The PA approximation of short-time diffusion properties is based on the cluster expansion of the N -particle translational mobility tensors of colloidal spheres,

$$\boldsymbol{\mu}_{ij}(\mathbf{X}) = \mu_0^t \mathbb{1} \delta_{ij} + \left[\boldsymbol{\mu}_{ij}^{(2)}(\mathbf{X}) - \mu_0^t \mathbb{1} \delta_{ij} \right] + \text{three-body terms} + \dots, \quad (58)$$

where the three-body and higher-order cluster contributions are disregarded. Here, $\mu_0^t = D_0^t / (k_B T)$ is the single-particle translational mobility coefficient depending on the hydrodynamic particle structure, and $\mathbb{1}$ is the unit tensor. The hydrodynamic mobility tensors on the pairwise additive level,

$$\boldsymbol{\mu}_{ij}^{(2)}(\mathbf{X}) = \mu_0^t \left[\delta_{ij} \left(\mathbb{1} + \sum_{l=1; l \neq i}^N \boldsymbol{\omega}_{11}(\mathbf{R}_{il}) \right) + (1 - \delta_{ij}) \boldsymbol{\omega}_{12}(\mathbf{R}_{ij}) \right], \quad (59)$$

with $\mathbf{R}_{ij} = \mathbf{R}_i - \mathbf{R}_j$, are fully accounted for including the near-contact lubrication terms. The two-particle tensors $\boldsymbol{\omega}_{11}$ and $\boldsymbol{\omega}_{12}$ describe the hydrodynamic self-interaction of a sphere through flow reflections at the second one, and cross-interactions of the two particles, respectively. The axial symmetry of the two-sphere problem allows for splitting these tensors into longitudinal and transversal components,

$$\boldsymbol{\omega}_{ij} = x_{ij}(r) \hat{\mathbf{r}} \hat{\mathbf{r}} + y_{ij}(r) [\mathbb{1} - \hat{\mathbf{r}} \hat{\mathbf{r}}]. \quad (60)$$

The transversal and longitudinal mobilities $x_{ij}(r)$ and $y_{ij}(r)$, with $i, j \in \{1, 2\}$, can be calculated recursively in the form of a power series in the reduced inverse pair distance a_h/r , combined with known near-contact lubrication expressions^{56,73,104}.

Insertion of Eq. (59) into Eq. (21) leads to the PA approximation expressions for D_S and $H_d(q)$ ⁴². We present these here in a form suitable for HRM particles where one distinguishes between the hydrodynamic particle diameter, $\sigma_h = 2a_h$, and the direct interaction diameter σ . For rigid spherical particles, $\sigma = 2a$ is the hard-core diameter, while for mechanically soft particles, σ is identified with a characteristic soft diameter σ_s such as the one in the Hertz potential.

Introducing the reduced length $x = r/\sigma_h$ and wavenumber $y = q\sigma_h$, the self-part contribution to $H(q)$ is

$$\left. \frac{D_S(\phi, \gamma)}{D_0^t(\gamma)} \right|_{\text{PA}} = 1 + 8\gamma^3 \phi \int_0^\infty dx x^2 g(\gamma x) [x_{11}(x) + 2y_{11}(x) - 3]. \quad (61)$$

The distinct part contribution reads

$$\begin{aligned} \left. H^d(y, \gamma) \right|_{\text{PA}} &= \gamma^3 \phi \quad (62) \\ &+ 18\gamma\phi \int_0^\infty dx x h(\gamma x) \left[j_0(xy) - \frac{j_1(xy)}{xy} + \gamma^2 \frac{j_2(xy)}{6x^2} \right] \\ &+ 24\gamma^3 \phi \int_0^\infty dx x^2 g(\gamma x) \bar{y}_{12}(x) j_0(xy) \\ &+ 24\gamma^3 \phi \int_0^\infty dx x^2 g(\gamma x) [\bar{x}_{12}(x) - \bar{y}_{12}(x)] \left[\frac{j_1(xy)}{xy} - j_2(xy) \right], \end{aligned}$$

where j_n is the spherical Bessel function of order n , and $h = g - 1$ is the total correlation function. The overlines in $\bar{x}_{12}(x)$ and $\bar{y}_{12}(x)$ indicate that the respective far-field parts up to third order in $1/x$ have been subtracted off. The argument γx in g and h , with $\gamma = \sigma_h/\sigma$, is a reminder that the RDF is commonly calculated as a function of r/σ such as in the VW-PY solution for hard spheres.

According to Eq. (61), the first-order virial coefficient of D_S is given by

$$\lambda_t(\gamma) = 8\gamma^3 \int_0^\infty dx x^2 \exp[-\beta V(x)] [x_{11}(x) + 2y_{11}(x) - 3]. \quad (63)$$

The PA approximation expression for the high-frequency limiting viscosity, generalized to the HRM reads,

$$\begin{aligned} \left. \frac{\eta_\infty(\phi, \gamma)}{\eta_0} \right|_{\text{PA}} &= 1 + \frac{5}{2} \gamma^3 \phi [1 + \gamma^3 \phi] \\ &+ 60 (\gamma^3 \phi)^2 \int_0^\infty dx x^2 g(\gamma x) J(x), \quad (64) \end{aligned}$$

with the rapidly decaying two-sphere shear mobility function, $J(x)$, accounting for the two-body HIs. It decays asymptotically as $J(x) \sim (15/128)x^{-6}$. We employ an accurate numerical table for $J(x)$ based on recursion expressions and the lubrication analysis given in Ref.¹⁰⁵.

Finally, we note that in the spherical annulus model of hydrodynamically structured hard spheres, the lower integration boundary of all integrals in the present appendix is equal to $1/\gamma$.

B Self-part corrected Beenakker-Mazur method applied to the HRM

Except for η_∞ , the applicability range of the PA approximation is restricted to lower ϕ values where it becomes accurate. In contrast, the $\delta\gamma$ -scheme for $H(q)$ and η_∞ by Beenakker and Mazur^{70,71} is applicable also to concentrated systems. We discuss here a standard version of this scheme, generalized to the HRM, where $S(q)$ is the only required input. Once the self-part D_S of $H(q)$ is suitably corrected^{42,106}, the $\delta\gamma$ method provides a decent description of short-time transport properties, for neutral and charge-stabilized particle systems alike (see Ref.⁴²). The $\delta\gamma$ method results for η_∞ and $H(q)$ reveal inaccuracies at all concentrations which can be partially attributed to its approximate treatment of the HIs. This is underlined in recent work by Makuch and Cichocki⁷² where the approximation steps in the derivation of the $\delta\gamma$ scheme have been reduced. The fact that their revised version of the $\delta\gamma$ scheme with improved hydrodynamic mobility tensors does not significantly improve the agreement with simulation data for no-slip hard spheres points to a fortuitous cancellation of errors introduced in the approximate derivational steps of the original (non self-part corrected) Beenakker-Mazur method.

A simple yet significant improvement over the original $\delta\gamma$ scheme preserving its analytical simplicity is obtained from using this scheme for the distinct part $H_d(q)$ only, where it gives overall good results. This was shown in Refs.^{42,67,106} both for neutral and charge-stabilized particle systems. Regarding the self-part, D_S , of $H(q)$, accurate expressions can be used instead such as the scaling relation in Eq. (26) for particles with hard-core interactions, or the PA approximation expression in Eq. (61) for lower-concentrated charge-stabilized systems. This hybrid procedure is referred to as the self-part corrected $\delta\gamma$ scheme.

The $\delta\gamma$ scheme expression for $H_d(q)$ by Beenakker and Mazur^{70,71}, generalized to the HRM, reads

$$H^d(y, \gamma) \Big|_{\delta\gamma} = \frac{3}{4\pi} \int_0^\infty dy' \left(\frac{\sin(\frac{1}{2}y')}{\frac{1}{2}y'} \right)^2 \frac{1}{1 + \gamma^3 \phi S_{\gamma_0}(\frac{1}{2}y')} \cdot \int_{-1}^1 d\mu (1 - \mu^2) \left[S\left(\frac{1}{\gamma} \sqrt{y^2 + y'^2 - 2yy'\mu}\right) - 1 \right], \quad (65)$$

with $y = q\sigma_h$. The function $S_{\gamma_0}(x)$ consists of an infinite sum of wavenumber-dependent contributions depending on ϕ_h as well as on the inter-related scalar coefficients $\gamma_0^{(n)}$, with $n \in \{0, 1, 2, \dots\}$. Explicit expressions for $S_{\gamma_0}(x)$ and $\gamma_0^{(n)}$ are given in Refs.^{66,70}. We have calculated the $\gamma_0^{(n)}$ coefficients in an iterative procedure up to $n = 10$, using a fine grid of volume fractions in $[0.01 - 0.5]$ of grid size $\Delta\phi = 0.01$. This has resulted in an improved accuracy as compared to the original

work by Beenakker and Mazur. However, the differences in $H_d(q)$ and η_∞ are quite small, i.e. there is no more than a 3% difference.

The $\delta\gamma$ scheme expression for η_∞ by Beenakker⁶⁹, adapted to the HRM, is given by

$$\frac{\eta_\infty(\phi, \gamma)}{\eta_0} \Big|_{\delta\gamma} = \frac{1}{\lambda^{(0)}(\phi, \gamma) + \lambda^{(2)}(\phi, \gamma)}, \quad (66)$$

where

$$\lambda^{(0)}(\phi, \gamma) = \left[1 + \frac{5}{2} \gamma^3 \phi \tilde{\gamma}_0^{(2)} \right]^{-1} \quad (67)$$

$$\lambda^{(2)}(\phi, \gamma) = \frac{15}{2\pi} \gamma^3 \phi \left[\tilde{\gamma}_0^{(2)} \lambda^{(0)}(\phi, \gamma) \right]^2 \int_0^\infty dy \frac{J_1^2(\frac{1}{2}y)}{1 + \gamma^3 \phi S_{\gamma_0}(\frac{1}{2}y, \gamma^3 \phi)} \left[S\left(\frac{y}{\gamma}\right) - 1 \right]. \quad (68)$$

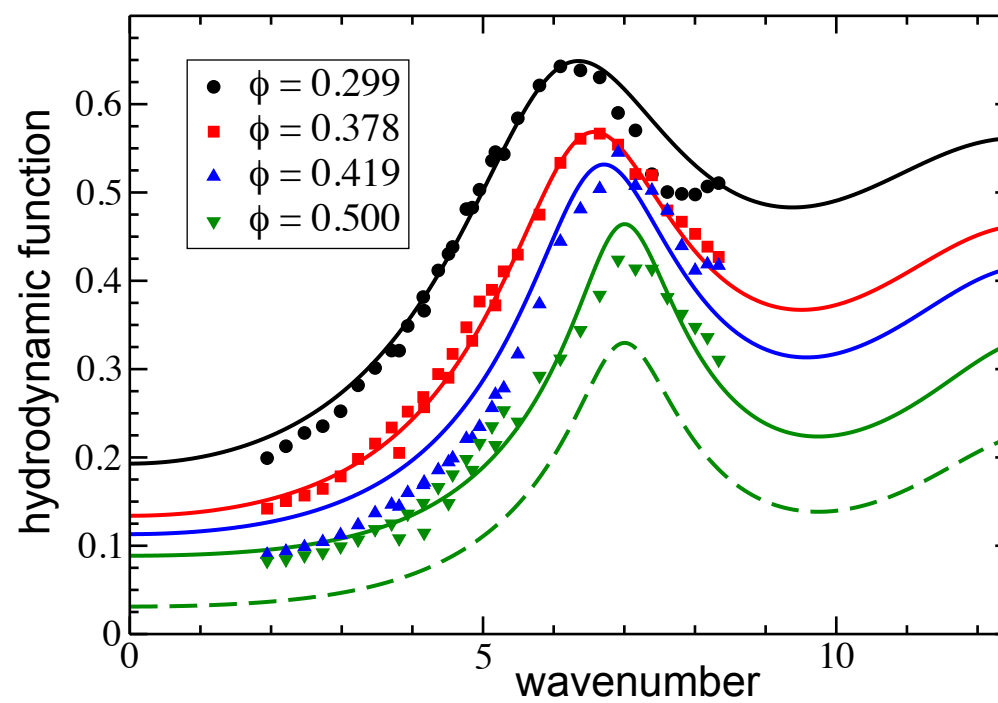
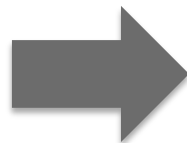
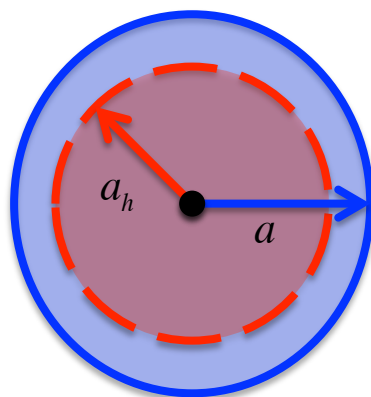
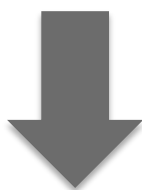
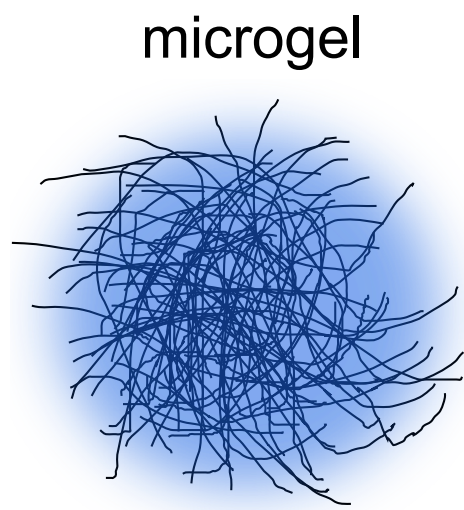
Here, $\tilde{\gamma}_0^{(2)} = \gamma_0^{(2)}/n$ with n denoting the particle number density. The argument y/γ in the static structure factor is used as a reminder that it is usually calculated as a function of $q\sigma$.

References

- 1 P. Holmqvist, P. S. Mohanty, G. Nägele, P. Schurtenberger and M. Heinen, *Phys. Rev. Lett.*, 2012, **109**, 048302.
- 2 G. M. Eichenbaum, P. F. Kiser, A. V. Dobrynin, S. a. Simon and D. Needham, *Macromolecules*, 1999, **32**, 4867–4878.
- 3 V. C. Lopez, S. Raghavan and M. Snowden, *React. Funct. Polym.*, 2004, **58**, 175–185.
- 4 N. Sahiner, C. Silan, S. Sagbas, P. Ilgin, S. Butun, H. Erdugan and R. S. Ayyala, *Microporous Mesoporous Mater.*, 2012, **155**, 124–130.
- 5 S. Lally, P. Mackenzie, C. L. LeMaitre, T. J. Freemont and B. R. Saunders, *J. Colloid Interface Sci.*, 2007, **316**, 367–75.
- 6 P. Panda, S. Ali, E. Lo, B. G. Chung, T. A. Hattton, A. Khademhosseini and P. S. Doyle, *Lab Chip*, 2008, **8**, 1056–61.
- 7 J. Shen, T. Ye, A. Chang, W. Wu and S. Zhou, *Soft Matter*, 2012, **8**, 12034.
- 8 S. Saxena, M. W. Spears, H. Yoshida, J. C. Gaulding, A. J. García and L. A. Lyon, *Soft Matter*, 2014, **10**, 1356–64.
- 9 K. Chari, R. Hsu, P. Bhargava, B. Figura, W. Yang, J. H. Park, T. Clifford and M. Kadir, *Langmuir*, 2013, **29**, 15521–8.
- 10 D. M. Heyes and A. C. Braka, *Soft Matter*, 2009, **5**, 2681.
- 11 R. Roa, E. K. Zholkovskiy and G. Naegle, in preparation.
- 12 W. Richard Bowen and P. M. Williams, *Chem. Eng. Sci.*, 2001, **56**, 3083–3099.
- 13 P. Debye and a. M. Bueche, *J. Chem. Phys.*, 1948, **16**, 573.
- 14 H. C. Brinkman, *Appl. Sci. Res.*, 1949, **1**, 27–34.
- 15 J. M. Deutch and B. U. Felderhof, *J. Chem. Phys.*, 1975, **62**, 2398.
- 16 B. Cichocki, M. L. Ekiel-Jezewska and E. Wajnryb, *J. Chem. Phys.*, 1999, **111**, 3265.
- 17 G. C. Abade, B. Cichocki, M. L. Ekiel-Jezewska, G. Nägele and E. Wajnryb, *J. Chem. Phys.*, 2010, **132**, 014503.
- 18 G. C. Abade, B. Cichocki, M. L. Ekiel-Jezewska, G. Nägele and E. Wajnryb, *Phys. Rev. E*, 2010, **81**, 020404.

- 19 G. C. Abade, B. Cichocki, M. L. Ekiel-Jezewska, G. Nägele and E. Wajnryb, *J. Chem. Phys.*, 2010, **133**, 084906.
- 20 G. C. Abade, B. Cichocki, M. L. Ekiel-Jeewska, G. Nägele and E. Wajnryb, *J. Phys. Condens. Matter*, 2010, **22**, 322101.
- 21 G. C. Abade, B. Cichocki, M. L. Ekiel-Jeewska, G. Nägele and E. Wajnryb, *J. Chem. Phys.*, 2012, **136**, 104902.
- 22 B. Cichocki, M. L. Ekiel-Jeewska and E. Wajnryb, *Colloids Surfaces A Physicochem. Eng. Asp.*, 2013, **418**, 22–28.
- 23 B. Cichocki, M. L. Ekiel-Jeewska and E. Wajnryb, *J. Chem. Phys.*, 2014, **140**, 164902.
- 24 G. C. Abade, B. Cichocki, M. L. Ekiel-Jeewska, G. Nägele and E. Wajnryb, in preparation.
- 25 J. L. J. Anderson, P. F. P. McKenzie and R. M. R. M. Webber, *Langmuir*, 1991, **7**, 162–166.
- 26 J. L. Anderson and Y. Solomentsev, *Chem. Eng. Commun.*, 1996, **148–150**, 291–314.
- 27 J. Riest, P. Mohanty, P. Schurtenberger and C. N. Likos, *Zeitschrift für Phys. Chemie*, 2012, **226**, 711–735.
- 28 D. Gottwald, C. N. Likos, G. Kahl and H. Löwen, *Phys. Rev. Lett.*, 2004, **92**, 068301.
- 29 B. Cichocki, M. L. Ekiel-Jeewska, G. Nägele and E. Wajnryb, *Phys. Fluids*, 2011, **23**, 083303.
- 30 M. G. McPhie and G. Nägele, *J. Chem. Phys.*, 2007, **127**, 034906.
- 31 G. Nägele, *Phys. Rep.*, 1996, **272**, 215–372.
- 32 C. N. Likos, *Microgel Suspens. Fundam. Appl.*, Wiley-VCH Verlag GmbH Co. KGaA, Weinheim, 2011, ch. 7, pp. 165–193.
- 33 D. Paloli, P. S. Mohanty, J. J. Crassous, E. Zaccarelli and P. Schurtenberger, *Soft Matter*, 2013, **9**, 3000.
- 34 G. C. Abade, B. Cichocki, M. L. Ekiel-Jeewska, G. Nägele and E. Wajnryb, *J. Chem. Phys.*, 2011, **134**, 244903.
- 35 M. Medina-Noyola, *Phys. Rev. Lett.*, 1988, **60**, 2705–2708.
- 36 J. F. Brady, *J. Chem. Phys.*, 1993, **99**, 567.
- 37 J. F. Brady, *J. Fluid Mech.*, 1994, **272**, 109.
- 38 A. J. Banchio, G. Nägele and J. Bergenholtz, *J. Chem. Phys.*, 1999, **111**, 8721.
- 39 A. R. Denton, *Phys. Rev. E. Stat. Phys. Plasmas. Fluids. Relat. Interdiscip. Topics*, 2000, **62**, 3855–64.
- 40 A. R. Denton, *Phys. Rev. E*, 2003, **67**, 011804.
- 41 J. K. Chung and A. R. Denton, *Phys. Rev. E*, 2013, **88**, 022306.
- 42 M. Heinen, A. J. Banchio and G. Nägele, *J. Chem. Phys.*, 2011, **135**, 154504.
- 43 T. Eckert and W. Richtering, *J. Chem. Phys.*, 2008, **129**, 124902.
- 44 J. C. Pàmies, A. Cacciuto and D. Frenkel, *J. Chem. Phys.*, 2009, **131**, 044514.
- 45 J. K. Percus and G. J. Yevick, *Phys. Rev.*, 1958, **110**, 1–13.
- 46 J.-P. Hansen and I. R. McDonald, *Theory of Simple Liquids, Third Edition*, Academic Press, 2006.
- 47 L. Verlet and J.-J. Weis, *Phys. Rev. A*, 1972, **5**, 939–952.
- 48 G. Nägele, *The Physics of Colloidal Soft Matter*, Institute of Fundamental Technological Research, Polish Academy of Sciences, Warsaw, Poland, Warsaw, 2004, p. 182.
- 49 H. Senff and W. Richtering, *J. Chem. Phys.*, 1999, **111**, 1705.
- 50 M. Stieger and W. Richtering, *Macromolecules*, 2003, **36**, 8811–8818.
- 51 C. N. Likos, M. Schmidt, H. Löwen, M. Ballauff, D. Pötschke and P. Lindner, *Macromolecules*, 2001, **34**, 2914–2920.
- 52 C. N. Likos, S. Rosenfeldt, N. Dingenouts, M. Ballauff, P. Lindner, N. Werner and F. Vögtle, *J. Chem. Phys.*, 2002, **117**, 1869.
- 53 B. Felderhof, *Phys. A Stat. Mech. its Appl.*, 1975, **80**, 63–75.
- 54 B. U. Felderhof and J. M. Deutch, *J. Chem. Phys.*, 1975, **62**, 2391.
- 55 C.-L.-M.-H. Navier, *Sur les lois du mouvement des fluides*, Mémoires de l'Académie Royale des Sciences de l'Institut de France, 6th edn, 1827.
- 56 S. Kim and S. Karrila, *Microhydrodynamics: Principles and Selected Applications*, Butterworth-Heinemann, Boston, 1991.
- 57 J. H. Masliyah, G. Neale, K. Malysa and T. G.M. Van De Ven, *Chem. Eng. Sci.*, 1987, **42**, 245–253.
- 58 M. Zackrisson, A. Stradner, P. Schurtenberger and J. Bergenholtz, *Phys. Rev. E*, 2006, **73**, 011408.
- 59 B. Cichocki and B. U. Felderhof, *J. Chem. Phys.*, 2009, **130**, 164712.
- 60 N. Lecoq, R. Anthore, B. Cichocki, P. Szymczak and F. Feuillebois, *J. Fluid Mech.*, 2004, **513**, 247–264.
- 61 D. Lopez and E. Lauga, *Phys. Fluids*, 2014, **26**, 071902.
- 62 G. Nägele, *Phys. Complex Colloids*, IOS Press, Proceeding edn, 2013, pp. 507–601.
- 63 E. Wajnryb, P. Szymczak and B. Cichocki, *Phys. A Stat. Mech. its Appl.*, 2004, **335**, 339–358.
- 64 H. Löwen, T. Palberg and R. Simon, *Phys. Rev. Lett.*, 1993, **70**, 1557–1560.
- 65 G. Nägele, M. Kollmann, R. Pesché and A. J. Banchio, *Mol. Phys.*, 2002, **100**, 2921–2933.
- 66 U. Genz and R. Klein, *Phys. A Stat. Mech. its Appl.*, 1991, **171**, 26–42.
- 67 A. J. Banchio and G. Nägele, *J. Chem. Phys.*, 2008, **128**, 104903.
- 68 M. Heinen, F. Zanini, F. Roosen-Runge, D. Fedunová, F. Zhang, M. Hennig, T. Seydel, R. Schweins, M. Sztucki, M. Antalík, F. Schreiber and G. Nägele, *Soft Matter*, 2012, **8**, 1404.
- 69 C. Beenakker, *Phys. A Stat. Mech. its Appl.*, 1984, **128**, 48–81.
- 70 C. Beenakker and P. Mazur, *Phys. A Stat. Mech. its Appl.*, 1984, **126**, 349–370.
- 71 C. Beenakker and P. Mazur, *Phys. A Stat. Mech. its Appl.*, 1983, **120**, 388–410.
- 72 K. Makuch and B. Cichocki, *J. Chem. Phys.*, 2012, **137**, 184902.
- 73 D. J. Jeffrey and Y. Onishi, *J. Fluid Mech.*, 1984, **139**, 261–290.
- 74 B. Cichocki and B. U. Felderhof, *J. Chem. Phys.*, 1991, **94**, 556.
- 75 M. Heinen, P. Holmqvist, A. J. Banchio and G. Nägele, *J. Appl. Crystallogr.*, 2010, **43**, 970–980.
- 76 M. Heinen, P. Holmqvist, A. J. Banchio and G. Nägele, *J. Chem. Phys.*, 2011, **134**, 129901.
- 77 M. Heinen, P. Holmqvist, A. J. Banchio and G. Nägele, *J. Chem. Phys.*, 2011, **134**, 044532.
- 78 C. C. Aburto and G. Nägele, *J. Chem. Phys.*, 2013, **139**, 134110.
- 79 W. T. Gilleland, S. Torquato and W. B. Russel, *J. Fluid Mech.*, 2011, **667**, 403–425.
- 80 W. B. Russel, *J. Chem. Soc. Faraday Trans. 2*, 1984, **80**, 31.
- 81 J. Phalakornkul, A. Gast, R. Pecora, G. Nägele, A. Ferrante, B. Mandl-Steininger and R. Klein, *Phys. Rev. E*, 1996, **54**, 661–675.
- 82 B. Cichocki and K. Hinsin, *Phys. A Stat. Mech. its Appl.*, 1992, **187**, 133–144.
- 83 P. Strating, *Phys. Rev. E*, 1999, **59**, 2175–2187.
- 84 D. R. Foss and J. F. Brady, *J. Rheol. (N. Y. N. Y.)*, 2000, **44**, 629.
- 85 T. N. Phung, *PhD thesis*, California Institute of Technology, Pasadena, California, 1993.
- 86 D. R. Foss and J. F. Brady, *J. Fluid Mech.*, 2000, **407**, 167–200.
- 87 A. J. Banchio and J. F. Brady, *J. Chem. Phys.*, 2003, **118**, 10323.
- 88 I. Moriguchi, *J. Chem. Phys.*, 1997, **106**, 8624.
- 89 M. D. Rintoul and S. Torquato, *Phys. Rev. Lett.*, 1996, **77**, 4198–4201.
- 90 W. van Meegen, S. M. Underwood and I. Snook, *J. Chem. Phys.*, 1986, **85**, 4065.
- 91 W. van Meegen and S. M. Underwood, *J. Chem. Phys.*, 1989, **91**, 552.
- 92 P. Segrè, S. Meeker, P. Pusey and W. Poon, *Phys. Rev. Lett.*, 1995, **75**, 958–961.
- 93 A. Weiss, N. Dingenouts, M. Ballauff, H. Senff and W. Richtering, *Langmuir*, 1998, **14**, 5083–5087.
- 94 R. A. Lionberger, *J. Rheol. (N. Y. N. Y.)*, 1997, **41**, 399.

-
- 95 R. A. Lionberger and W. B. Russel, *Adv. Chem. Phys.*, John Wiley & Sons, Inc., Hoboken, NJ, USA, 1999, vol. 111, pp. 399–474.
- 96 G. Nägele and J. Bergenholtz, *J. Chem. Phys.*, 1998, **108**, 9893.
- 97 B. Cichocki and B. U. Felderhof, *J. Chem. Phys.*, 1990, **93**, 4427.
- 98 G. Nägele and P. Baur, *Europhys. Lett.*, 1997, **38**, 557–562.
- 99 M. Rex and H. Löwen, *Eur. Phys. J. E. Soft Matter*, 2009, **28**, 139–46.
- 100 P. Segrè and P. Pusey, *Phys. Rev. Lett.*, 1996, **77**, 771–774.
- 101 P. Holmqvist and G. Nägele, *Phys. Rev. Lett.*, 2010, **104**, 058301.
- 102 K. Zahn, J. Méndez-Alcaraz and G. Maret, *Phys. Rev. Lett.*, 1997, **79**, 175–178.
- 103 B. Rinn, K. Zahn, P. Maass and G. Maret, *Europhys. Lett.*, 1999, **46**, 537–541.
- 104 R. Jones and R. Schmitz, *Phys. A Stat. Mech. its Appl.*, 1988, **149**, 373–394.
- 105 D. J. Jeffrey, *Phys. Fluids A Fluid Dyn.*, 1992, **4**, 16.
- 106 F. Westermeier, B. Fischer, W. Roseker, G. Grübel, G. Nägele and M. Heinen, *J. Chem. Phys.*, 2012, **137**, 114504.



Analytic toolbox

An analytic toolbox is presented for the calculation of short-time and long-time transport properties of hydrodynamically structured particles suspensions.